Field Guide

1. TVZ introduction

Volcanism

Geothermal activity

2. White Island composite volcano

Introduction

Historical activity

3. Okataina Volcanic Centre

Introduction

Tarawera

1886 eruption

4. Tongariro composite volcano

Introduction

Ngauruhoe (Mt Doom)

1975 Ngauruhoe eruption

5. Ruapehu composite volcano

Introduction

Ruapehu 1995-96

2007 lahar threat

White Island

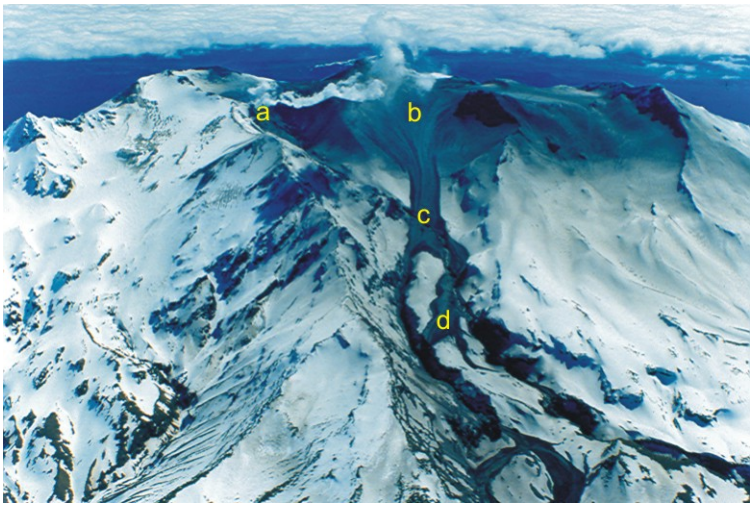

Ruapehu 1995 Lahars

Tarawera

6. Taupo Volcanic Centre

Introduction

Taupo 181 AD

Plinian phases

Phreatoplinian phases

Taupo Ignimbrite

Sedimentary response/aftermath

Separate volume: Route Guide

Ruapehu September 1995

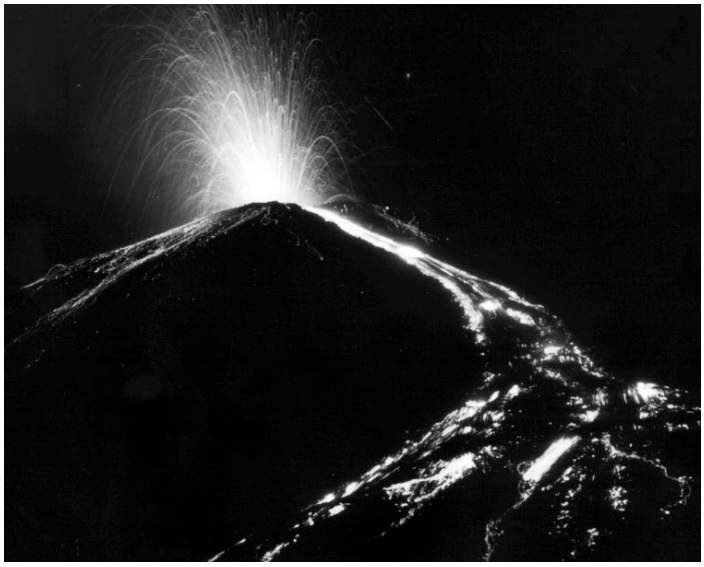

Ngauruhoe 1955 Eruption

Taupo caldera (cone volcanoes in background).

1. TVZ introduction

The New Zealand landmass, including the North, South, and outlying islands, is part of a larger submerged microcontinent that originally formed on the eastern margin of the Gondwanaland supercontinent. It separated from Gondwanaland during the Late Cretaceous. North of New Zealand, the rotating Pacific plate drops down the Kermadec trench, and collides head on with the Australian plate (Figure 1.1). Eastern New Zealand is dragged down the subduction zone and south, to a limited extent by friction, explaining why the North Island is tending to split apart to form the triangular Taupo Volcanic Zone. Since the Euler pole is close to New Zealand, rotation of the Pacific Plate here is fairly slow around short radii. This explains how a "rigid" Pacific Plate has different velocities. In the middle of New Zealand, relative plate motion between the Pacific and Australian plates converts towards sliding along multiple fault lines. The trench becomes shallow and ill defined. Further south again, the rotating Pacific plate is sliding south relative to the Australian plate defining the spectacular Alpine Fault (Figure 1.1).

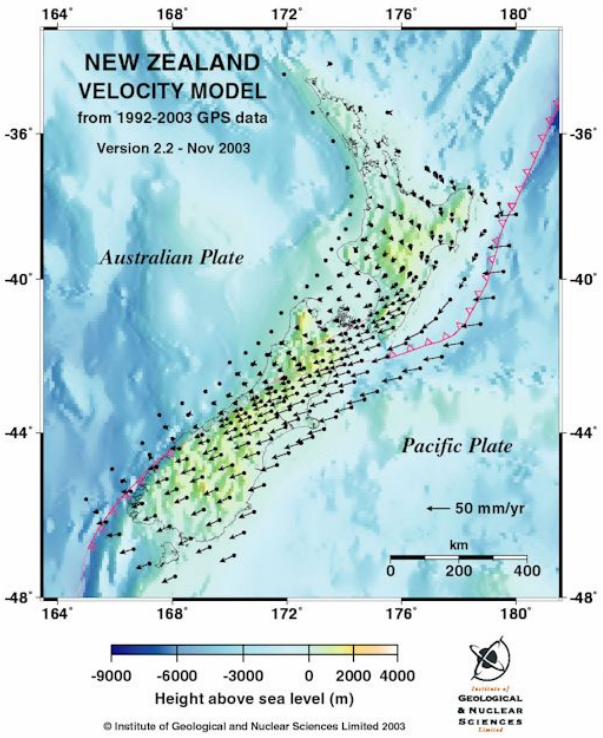

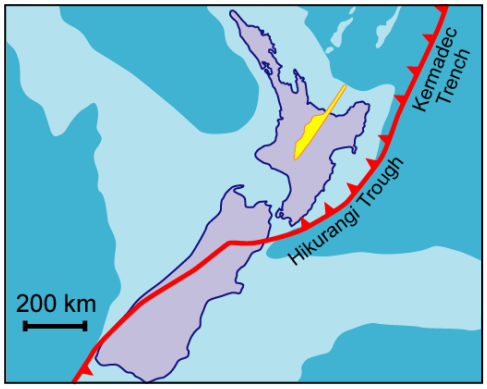

Figure 1.1: Left: Plate velocity model for New Zealand constructed by John Beavens.
Right: The Taupo Volcanic Zone (in yellow) actively Rifting due to the relative
Motion of the Pacific and
Australian plates.

Taupo Volcanic Zone contains most of the Quaternary volcanism in New Zealand (Figure 1.2). TVZ is a rifted arc, but its segmented nature, high thermal flux and voluminous rhyolitic volcanism make it unique on Earth. TVZ is a volcano-tectonic complex, 300 km long and up to 60 km wide, defined by an envelope around all vent locations known or inferred to have been active during the past 2.0 m.y. and associated with a northeast structural trend (Wilson et al, 1984). Andesitic activity started at c. 2 Ma, joined by voluminous rhyolitic (plus minor basaltic and dacitic) activity from c. 1.6 Ma (Houghton et al. 1995).

Volcanism

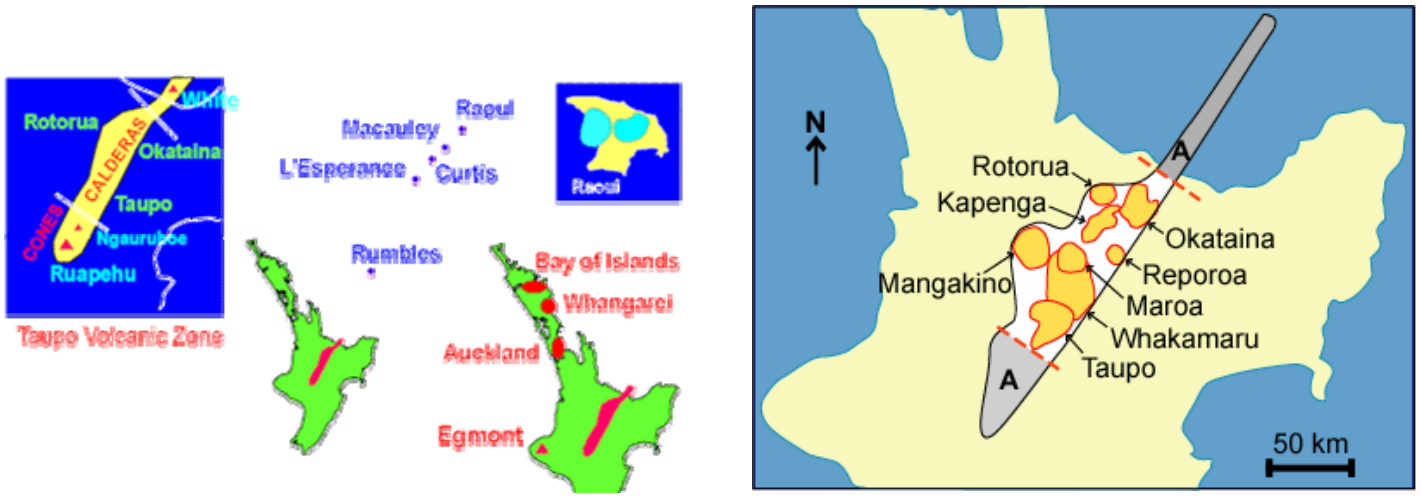

Figure 1.2: Active volcanoes of New Zealand, with an emphasis on Taupo Volcanic Zone. Note the three-fold division of the zone into regions dominated by either composite cones (andesite) or by rhyolitic calderas (in yellow). After Brad Scott

TVZ shows a pronounced segmentation into NE and SW andesite-dominated extremities with composite cones and no calderas, and a central 125-km-long rhyolite-dominated segment. Rhyolite (> 15 000 km3 bulk volume, typically 70-77% SiO2) is the dominant TVZ magma (mostly as caldera-forming ignimbrite eruptions), andesite is an order of magnitude less abundant, and basalt and dacite are minor in volume (<100 km3 each). Central Taupo Volcanic Zone is the most frequently active and productive silicic volcanic system on Earth, erupting rhyolite at c. 0.28 m^3 s-1 (Houghton et al., 1995; Wilson et al. 1995). The rhyolites show no major compositional changes with time, but the total range of magma chamber zonation has narrowed with the advent of rifting and crustal extension at c.0.7 Ma. At least 34 caldera-forming ignimbrite eruptions have formed a complex sequence of relatively short-lived, nested and/or overlapping volcanic centers in central TVZ. Taupo contrasts with other large silicic magmatic systems in the exceptionally high frequency, but small size, of caldera-forming eruptions.

This contrast reflects the thin, rifted nature of the TVZ crust, which precludes the development of long-term magmatic cycles at Taupo. Within central TVZ, non-rhyolitic compositions have been erupted apparently irregularly in time and space; in particular there is no evidence for a geographic separation of basalts from andesites. Central TVZ is a broad structural depression, with a regional negative gravity anomaly, which contains local anomalies of 20-40 mgal, reflecting caldera centres and tectonic basins (e.g. Rogan, 1982). Mesozoic and Tertiary marine sedimentary rocks flank most of TVZ, and ignimbrites extend >50 km from their sources on both sides of the zone. Calculations based on gravity data (e.g. Rogan, 1982) suggest thicknesses of volcanic material of at least 2.5-3 km and a total volume of volcanic material in the central TVZ of 10 000-12 000 km^3. When allowance is made for pyroclastic deposits outside the zone, a total minimum volume of 15 000-20 000 km^3 of volcanic material is likely to have erupted.

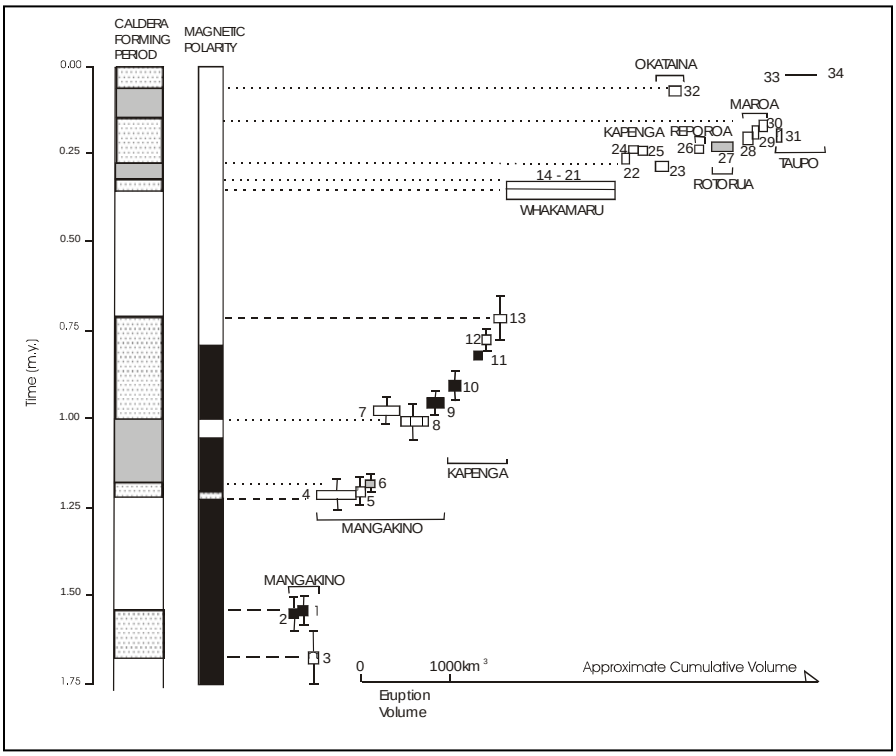

Figure 1.3: age of caldera forming eruptions in TVZ. *After Houghton et al. 1995)*

Taupo Volcanic Zone and the Yellowstone system are used as archetypal examples of large caldera volcanoes (e.g. Smith and Bailey, 1968). Their averaged magma discharge rates and total thermal fluxes are very similar, suggesting magma supply rates are comparable, despite their disparate tectonic settings. These supply and discharge rates are high in comparison to other silicic caldera systems and similar to frequently active composite cones. However the styles, sizes and frequencies of eruptions are strikingly different at Yellowstone and TVZ (Figure 1.1) and we suggest that this is a function of the age, strength and deformation characteristics of the crust in the two regions. There is a comparatively simple history of three long-term magmatic cycles over the past 2.2 m.y. at Yellowstone, each culminating in voluminous ignimbrite eruptions and caldera collapse (Christiansen, 1984). In this stable continental setting, large magma chambers can evolve over extended time intervals (10^5 to 10^6 years), and the life span of individual magma batches is long. In contrast, central Taupo Volcanic Zone has formed at a convergent margin where the crust is younger, thinner, and undergoing rapid extension at up to 18 mm year-1. Thus in TVZ relatively small caldera-forming events occur relatively frequently from a cluster of nested or overlapping volcanic centres that experience magmatic cycles which are disrupted on time scales of 10^4 to 10^5 years.

Geothermal activity

A *geothermal system* is a region of the earth where the rocks have been raised naturally to higher temperatures than surrounding regions. Active volcanoes are regions of unusually high heat flow and, not surprisingly, many geothermal systems are associated with young volcanoes. We see, in TVZ, a strong link between the major rhyolitic volcanoes and large geothermal systems. Within a geothermal system heat is transferred partly through the rock itself (conduction) and partly by the movement of hot water (convection). Up to 50 % of the heat released at the surface may be transported by hot water, and water chemistry shows that most of that water was originally atmospheric rain. This cold rainfall moves downwards

through cracks and cavities in the surface rocks towards a heat source deep within a geothermal system, absorbing heat and becoming progressively hotter. This hot water is less dense than cold water, and, if there is access to the surface, the hot water rises and ultimately discharges as geysers, hot springs, and fumaroles. The three requirements for geothermal activity are therefore water, heat, and rapid passage to the surface. Where these coincide a geothermal field occurs. It may take several years or even tens of years to go through a complete cycle from rain falling on the surface, through deeply circulating groundwater, to the water re-emerging at the surface in springs.

Areas of hot springs are generally only a small part of the total geothermal system. The hot spring areas frequently occur along faults or are in topographic low points where water levels are near the surface (Figure 1.4). Fault lines provide a convenient escape route for hot geothermal water, e.g., the three fields of hot springs in Rotorua basin— Tikitere, Whakarewarewa, and Ohinemutu—are all related to faults. The total geothermal system at depth however is commonly a much larger area, and includes impermeable regions with no evident surface geothermal activity.

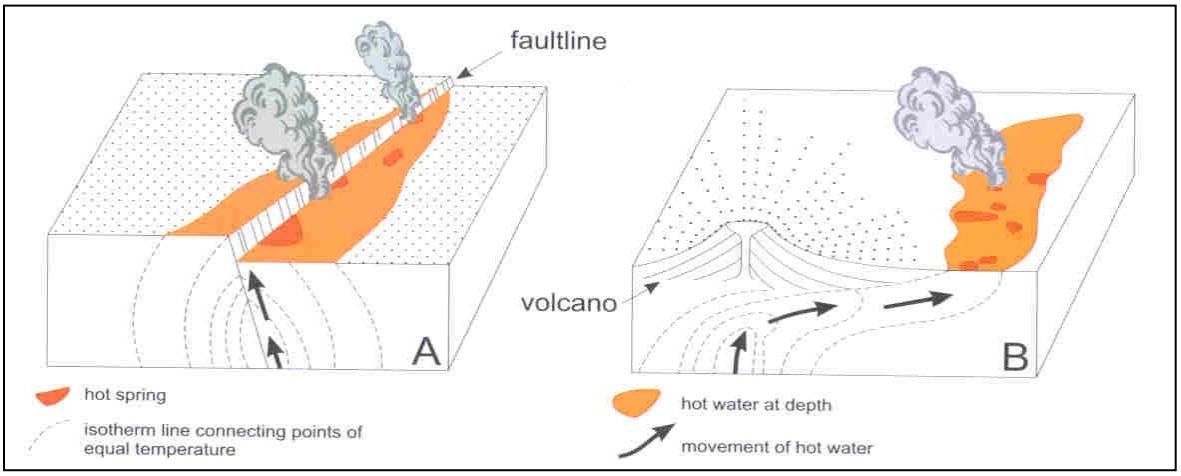

Figure 1.4: Geothermal activity is related to geological structure. A springs commonly align with fault traces and b. geothermal fields often occur at low elevation on the flanks of a cone.

Activity in geothermal systems includes *geysers*, *hot springs*, *mud pools*, and *fumaroles*. Geysers and hot springs occur where geothermal water, rising along a zone of weakness, such as a fault, has rapid access to the surface. The result is rapid, free discharge of hot water. The discharged water varies markedly in composition from surface water, mainly due to chemical interaction with rock on its way to the surface. Water discharged by hot springs is typically weakly alkaline, and as it is rich in sodium and particularly *chloride*, it is called alkaline chloride water. Geysers are a special class of boiling hot springs, with intermittent jets of water and steam. Many hot springs lose heat to the atmosphere and surrounding rock at the same rate at which heat enters from below, and so the springs discharge hot but not boiling water. Most geysers, however, have a narrow vent opening to a substantially larger reservoir below the surface (Figure 1.5). The narrow neck of geysers reduces surface heat loss from the system, so water in the reservoir increases steadily in temperature until it begins to boil. A mixture of steam and water is then violently ejected. When the supply of boiling water is exhausted, the discharge ceases and the reservoir begins to recharge. The recharge period, and thus the time between eruptions, depends on the reservoir size and the rate of

transfer of heat. If the vent of a geyser is modified, it is often sufficient to stop it erupting. Geysers have a limited life and they remain rare and precious.

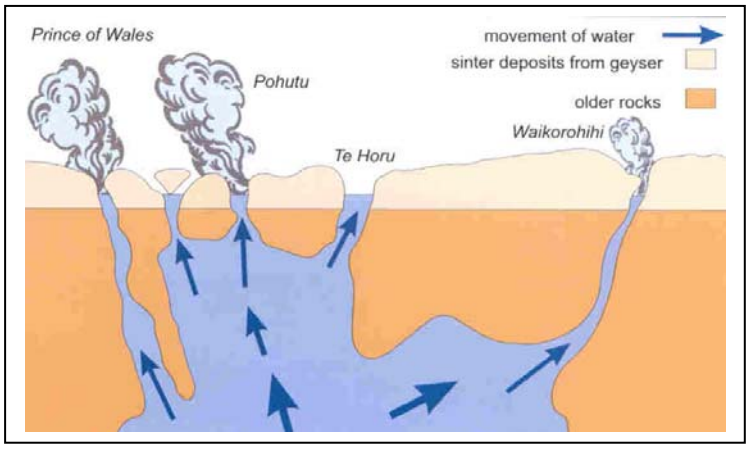

Figure 1.5: Model for the geothermal plumbing system at Whakarewarewa.

In other areas similar water reaches close to the surface but is then trapped at shallow levels by aquicludes that it cannot penetrate. The trapped water may boil at depth, with steam and gas escaping to the surface through a fumarole. The rising steam and gas may react with surface water and soil to form a mud pool. Because the mixture of gas and water is trapped at shallow level for some time, it may react chemically with the soil, altering its composition. Hydrogen sulphide may oxidize to form sulphuric acid and the resulting waters are known as acid sulphate waters. We can therefore contrast geysers and hot springs discharging alkaline chloride waters on one hand with fumaroles and mud pools discharging acidic sulphate waters on the other.

Geothermal water contains a wide range of dissolved chemical compounds. A number of gases, notably carbon dioxide and hydrogen sulphide, are also held in solution and released when the water approaches the surface. The striking geothermal deposits familiar to any visitor to the Rotorua district are the result of reaction between the compounds in solution in the cooling geothermal water as it approaches the surface and the near surface and surface rocks and water. Sinter precipitates from cooling geothermal water, and is usually composed of hydrous silica (or silicon dioxide, SiO_2), Progressively more silica can be dissolved as the temperature of the water is increased and conversely, if the water cools, silica must precipitate. The rate of silica crystallization is very rapid and so *common opal*, a form of silica where the atoms are in rather random distribution, generally forms, rather than quartz, which has atoms in a very well organized, tightly bound framework. Small amounts of other compounds or elements can be incorporated into the sinter, tinting the normally white silica. Pyrite (FeS_2) impurities produce a dark grey coloration (e.g. around Kereru Geyser at Whakarewarewa), while ferric iron oxides (Fe_2O_3) produce a pink color (e.g. around Pohutu Geyser). Algal growth on a silica terrace is often responsible for a range of green, brown, and black colors.

2. White Island composite volcano

Background

White Island is currently New Zealand's most frequently active volcano. Situated 48 km offshore in the Bay of Plenty, its activity is often clearly visible to inhabitants of the surrounding region. The island was the scene of one of the three major volcanic disasters in New Zealand when 11 sulfur miners were killed there in 1914. Since 1976, White Island has been more active than at any other time in the last few hundred years, and has aroused considerable public interest in the level of volcanic hazard it presents.

Figure 2.1: Aerial view of White Island showing the composite crater with activity focused in the western sub-crater.

White Island is the summit of a large (16 x 18 km) submarine composite volcano which has grown up from the sea floor at 300 to 400 m depths. Only half the height and very small proportion of the volume of this volcano are above sea level. The main crater (Figure 2.1) was formed in prehistoric times, apparently by the coalescence of three overlapping roughly circular sub-craters. The eastern sub-crater was formed first, and now contains only minor hot spring activity. The western sub-crater contains most of the eruption sites that have formed since 1960 and has been the main focus of activity during the island's recorded history. Deep pits mark the sites of recently active vents. Most of the present main crater floor lies less than 30 m above sea level, and has an irregular surface covered by mounds of avalanche debris from the 1914 disaster.

Activity at White Island as far back as 16,000 years ago is recorded by volcanic ash layers found in ocean floor sediment drill cores, but the island was undoubtedly active long before this time. The ocean floor core data provide the only presently available record of the prehistoric activity of White Island, as no old ash deposits from the volcano have yet been identified on the North Island.

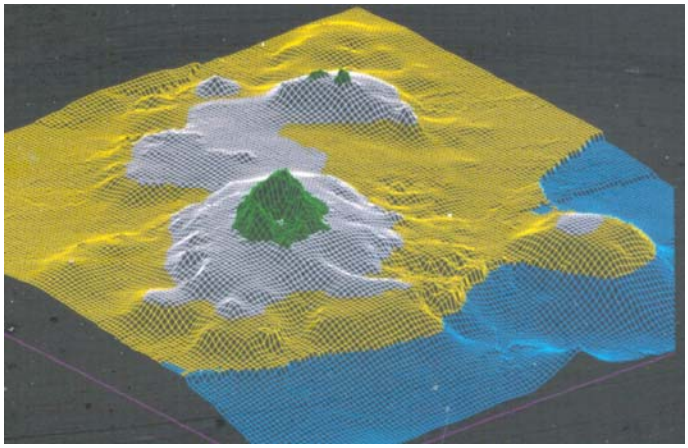

Figure 2.2: Only half the height and a very small proportion of the volume of White Island are above sea level. This digital elevation map by Brad Scott shows very clearly the full extent of the cone and also that Volker rocks and Club rocks (top of the image) are simply emergent parts of the early portions of the composite structure.

Figure 2.3: The tripartite form of the main crater is clear in these two vertical images and also the focus of the current activity close to the junction of the western and central subcraters in the 1978-90 crater complex. This crater-in-crater-in-crater geometry reflects the weak unconsolidated nature of the vent and conduit walls.

Figure: 2.4 Mapping by Thor has shown that the subaerial volcano consists of two superimposed cones- an older Ngatoro cone to the west has superimposed on its flanks the modern central cone. If we circumnavigate the island we will see the numerous andesite-dacite lava flows which are the "building blocks" for the inner and outer walls of the cones (see below).

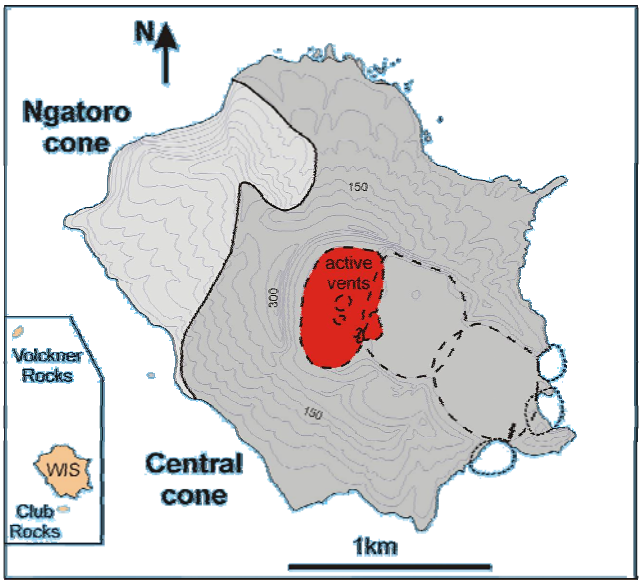

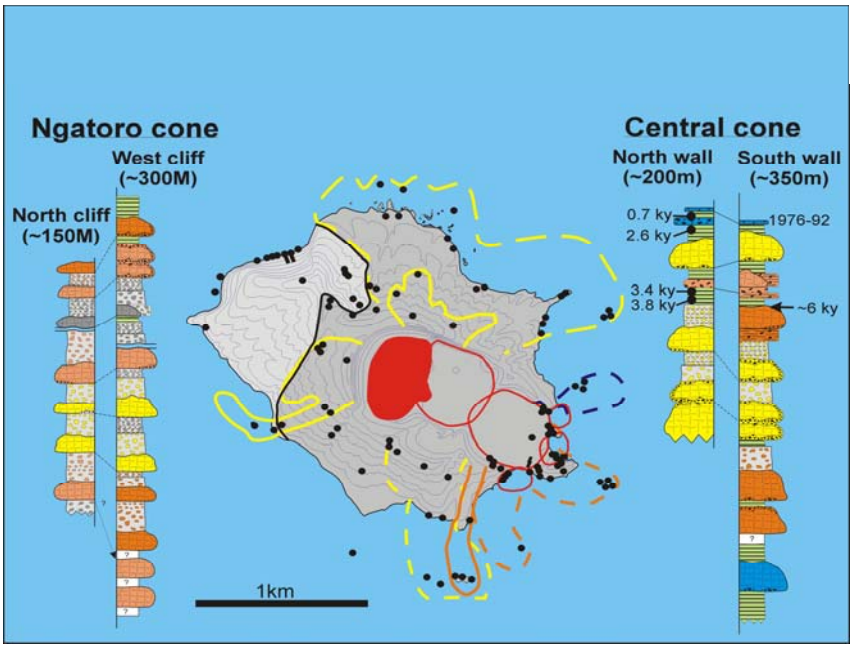

Figure 2.5: Here are four of Thor's measured sections showing the alternation of sheet lava and autobreccia that you will become very familiar with at Tongariro. The lobate form of the youngest lavas and their valley-confined nature are very clear from the map. Note that the youngest flows clearly extend well below modern sea level.

Historical activity

The written history of White Island observations begins in 1826; since then a state of continuous low level activity with intermittent small eruptions has been recorded. The crater floor was often flooded by hot lakes, until these were permanently drained in 1913 so that sulfur deposits on the crater floor could be mined. In September 1914 the southwest corner of the high crater wall collapsed to produce a hot avalanche which buried 11 sulfur miners and destroyed buildings and equipment at the eastern end of the crater (Figure 2.2).

Figure 2.6: Debris avalanche mounds from the 1914 sector collapse. Source is near the lower point on the skyline to the left.

Since 1914 new vents have formed in the west and central sub-craters, associated with small steam and ash eruptions. "1933 Crater" formed in that year during an explosive ash eruption; "Noisy Nellie Crater" formed prior to January 1947; "Big John Crater" grew to 50 m diameter during eruptions between 1962 and 1965. A steam and ash eruption in November 1966 accompanied formation of the 60 m diameter, 120 m deep new vent "Gilliver Crater". Rudolf vent grew from a fumarole during ash eruptions in 1968, to reach 45 m diameter and 120 m depth by 1969. Some ash fell on the North Island during these eruptions. Two years later, a single explosive eruption formed "1971 Crater".

1976-1982 eruption cycle

No further eruptive activity occurred between 1972 and December 1976, when the largest and longest sequence of eruptions recorded at White Island began and continued until the beginning of 1982. These eruptions were caused by the rise of molten rock (magma) beneath the volcano, to reach shallowest levels in 1977 and 1978, when the largest individual eruptions occurred and incandescence (glows) could be seen at night from the Bay of Plenty coast. Lava bombs and blocks (see box) were erupted and voluminous ash clouds rose above the island. The "1978 Crater Complex" was formed by collapse and explosive excavation around the active vents (Figure 2.3). Fine ash fell on the Bay of Plenty coast on several occasions during the 1976-1982 period, but this ash was quickly removed by wind and rain and is not preserved. At times the floor of the vent was more than 200 m below sea level.

The end result of the 1976-1982 activity was the partial re-excavation of the sediment-filled prehistoric western sub-crater, and the deposition of about 10^7 cubic meters of volcanic ash on the island and offshore. All the individual eruptions during the 1976-1982 period rate as "small" (less than 1 million cubic meter) on the world scale of eruption sizes. A significant hazard existed on and immediately adjacent to the island on only a few days of the entire active period. At no time was the Bay of Plenty coast significantly affected, apart from a few days of ash contamination of roof collected tank water supplies in the eastern Bay of Plenty.

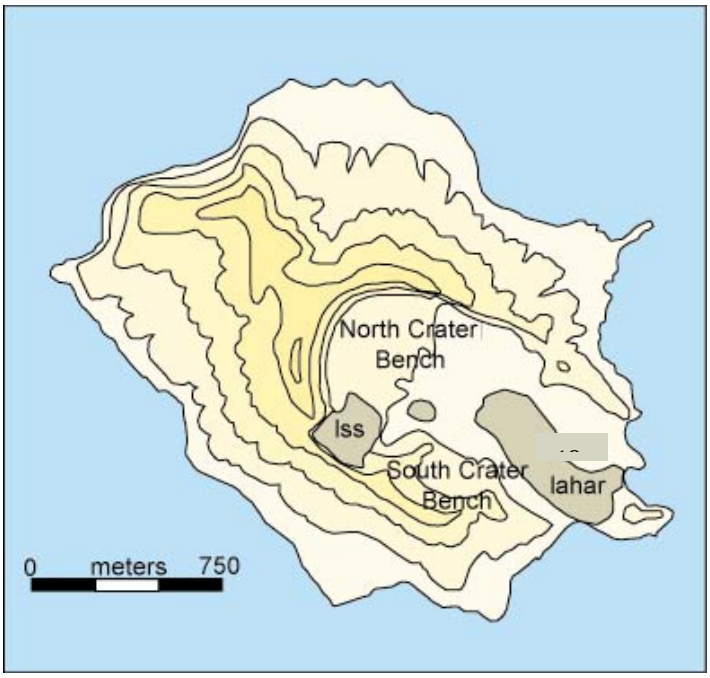

Figure 2.7: Topographic map of White Island, prior to 1976. North Crater Bench is now subsumed by the 1976-90 crater complex. Iss is the site of the 1914 collapse and the deposits are shown in grey.

Recent activity

A similar, but less intense, and less well-studied series of eruptions took place between February 1986 and May 1992. The crater complex formed in 1976-1982 was enlarged during a sequence of predominantly phreatomagmatic and infrequent Strombolian explosions. Phreatomagmatic plumes were short lived but occasionally rose to heights of 3 to 7 km ejecting ballistic blocks and forming fall and surge deposits.

Since 1992 explosive activity has occurred more intermittently. Rare larger explosions until 2006, e.g. in 1998 have deposited fine ash as far as the North Island.

Currently a large lake has formed in the crater complex and reached close to overflow levels. This has had the effect of quenching much of the superficial geothermal activity in the crater complex. The crater lake has continued to heat and reached 74 degrees C on 22 February 2007, the highest recorded temperature. Because the lake is so hot, steam plumes are now often seen over the island. The water level of the lake is now dropping as the lake evaporates.

White Island explosions are always unpredictable and phreatomagmatic explosions have few if any precursors and can eject blocks to distances of hundreds of meters from the vent. The island also has an unhealthy flux of volcanic gas including sulfur species. We will take a cautious approach to the volcanology.

3. Okataina Volcanic Centre

Introduction

The Okataina Volcanic Centre was previously linked by Nairn (1981, 1989) to eruption of 4 ignimbrites, but current models definitely attribute only the 0.28±0.01 Ma Matahina Ignimbrite (Bailey and Carr, 1994; date from Houghton et al., 1994) and 65 ka Rotoiti eruption (Nairn, 1981, Davis, 1985, Wilson et al., 1992) to caldera collapses at this centre. Okataina, along with Taupo, remains highly active (average 0.08 m3 s-1 over the past 65 ka) and is among the most productive rhyolite volcanoes documented.

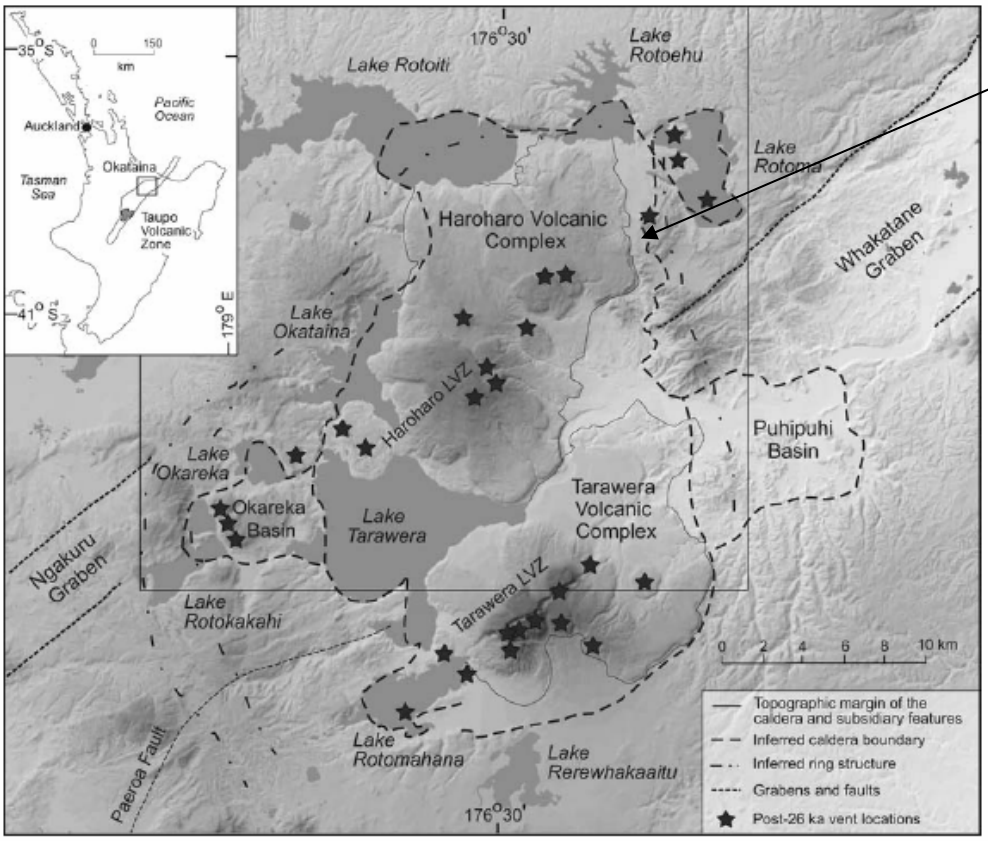

Figure 3.1: Outline of Okataina and adjacent Rotorua volcanic centres. Note cuspate form of topographic margin of caldera and the alignment of post 20 ka vents (stars) which cross Tarawera (south) and Haroharo (north) dome complexes.

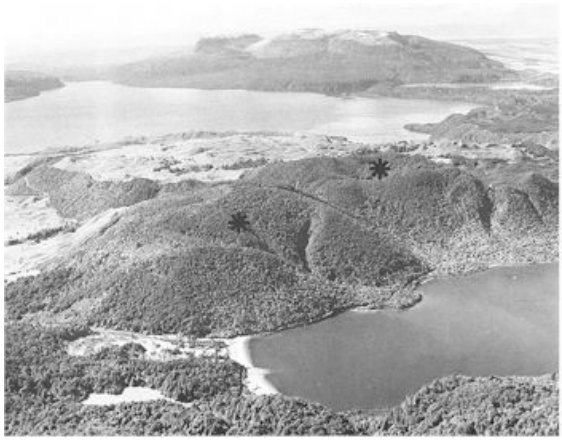

Figure 3.2: Haroharo (foreground) and Tarawera dome complexes.

Post-caldera activity at Okataina contrasts with Taupo in that there have been fewer but generally larger eruptions, often with substantial volumes of lava that have largely filled the younger caldera structure. Two large dome complexes Tarawera and Haroharo have grown to occupy much of the caldera over the last 20 ka (Fig. 3.2). The most recent activity was at Tarawera in 1886 AD (the largest known TVZ basalt eruption) and 1314 AD (the youngest TVZ rhyolite eruption).

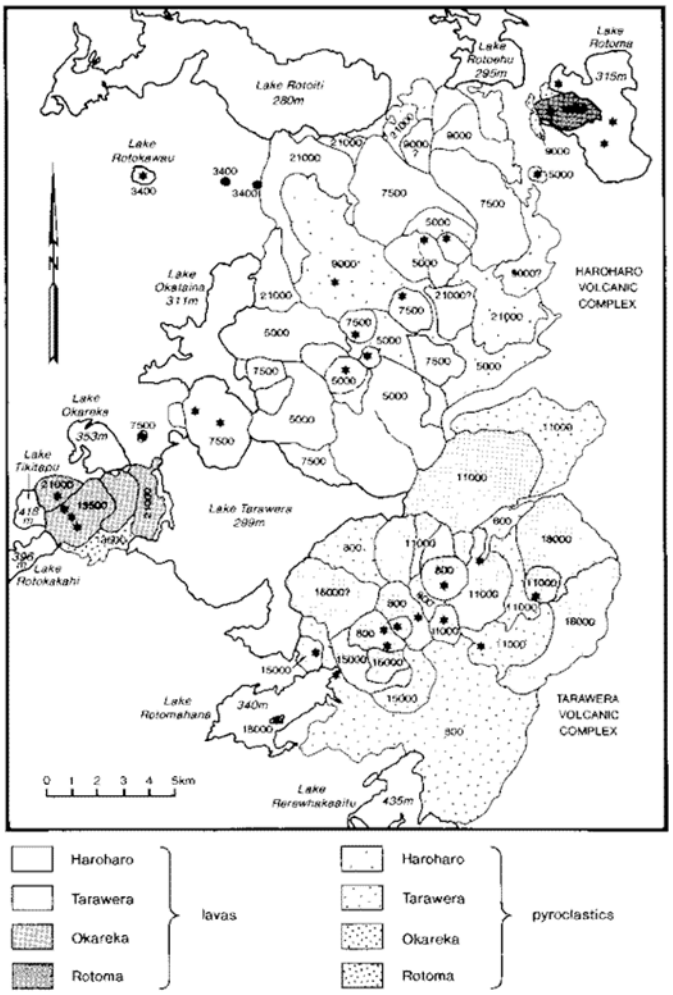

Figure 3.3 Ages of young lava domes and flows at Okataina. *After the work of I.A. Nairn.*

Tarawera dome complex

Tarawera was the locus of rhyolitic eruptions at 18000, 15000, 11000 and 700 (1314 AD) 14C years ago as well as the site of vents of the 1886 eruption (Cole, 1970; Nairn and Cole, 1981). Small volumes of basalt were erupted during two of the four rhyolitic eruptions (Leonard et al., 2002). During the Kaharoa eruption four summit lava domes (Fig. 3.3) were extruded and voluminous block and ash flows were generated by the collapse from the margins of the growing domes (Nairn et al., 2001). These domes define Mt Tarawera and establish the surface 'architecture' of the vent region for the 1886 eruption (Fig. 3.2) The Kaharoa domes and pyroclastic deposits represent a major, easily identified source of wall-rock lithic clasts in the 1886 deposits, which played a key role during the eruption.

The 1886 eruption

The 1886 eruption of Tarawera volcano in the Taupo Volcanic Zone was New Zealand's largest and most destructive historical eruption (Walker et al. 1984). This event was unusual in several ways. First, although the eruption involved exclusively basaltic magma, its main phase included intense sustained activity that is rarely associated with basalt, resulting in a >10,000 km^2 plinian fall deposit (Thomas 1888; Walker et al. 1984). Second, the eruptive source was a 17-km-long fissure (Fig. 3.4) formed by >50 vents in thirteen major craters across Mt Tarawera itself (Fig. 3.5 in addition to as an uncertain number of vents to the southwest at Rotomahana (Nairn 1979; Nairn and Cole 1981; Houghton et al. 2004a). Third, in addition to the plinian sheet of scoria fall (Fig. 3.6), the eruption produced strongly over-thickened proximal deposits on Mt Tarawera that form a series of half-cones on both sides of the fissure (Fig. 3.7), visible in excellent exposures at sites extremely close (90-300 m) to vent (Houghton and Wilson 1998). The geometry of the 1886 proximal deposits is extremely complex and has consequent implications for the diversity of transport and deposition processes not only for the Tarawera eruption itself but also for plinian plumes in general. Tarawera 1886 provides a valuable opportunity to study links between fall deposition close to vent and deposition in the far field. About 0.8 km^3 of basaltic magma (DRE) was erupted in only five and a half hours (Walker et al. 1984). This eruption deposited scoria up to 150 km, and ash up to 230 km downwind, to the northeast (Thomas 1888).

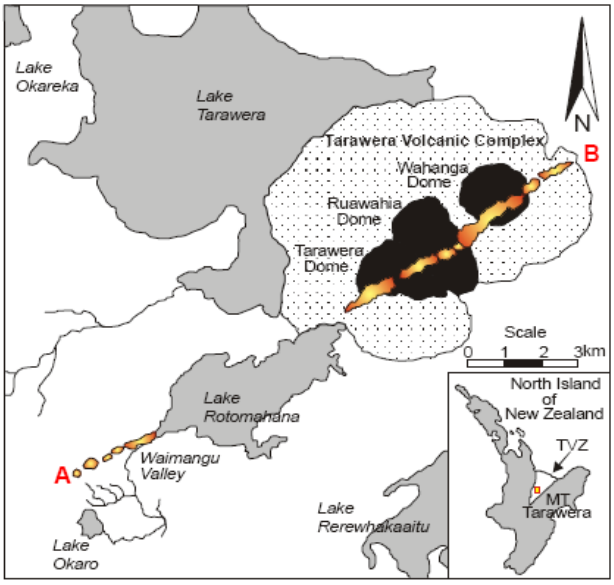

Figure 3.4: Location map. 1886 eruption fissure (AB) extends 17 km from the Waimangu geothermal field to Mt Tarawera. Modern Lake Rotomahana occupies at least 5 coalesced craters from the 1886 eruption. 1314 Kaharoa lava domes are shown in black. Older domes are stippled.

Chronology

Minor precursory activity included an increase in geothermal activity occurred at Lake Rotomahana and a 30 cm high wave on Lake Tarawera, early on the morning of 1 June 1886, which has been interpreted to have been caused by ground movement (Nairn, 1979).

The most significant precursors were felt earthquakes which began one hour prior to the onset of the eruption on 10 June 1886. These earthquakes increased in intensity before the first outbreak (Nairn 1979), which began at 0130 (local time), in the vicinity of Wahanga, the northeastern-most of the Kaharoa domes (Fig. 3.5).

Shortly after 2:00 a.m., ash columns were observed above two pre-existing lava domes on Mt Tarawera, identified by eyewitnesses as Wahanga and Ruawahia domes (Fig. 3.4; Williams 1887). Activity spread both northeast and southwest to form an 8-km-long chain of 13 elongate craters separated by septae where the dikes did not break the surface (Nairn and Cole 1981; Walker et al. 1984). Sustained eruption produced a curtain of fountains and a plume described as more than 10 km high (Keam 1988). At 2:30 a.m. a second plume rose from a vent farther to the southwest, widely assumed to be due to initial explosions at Rotomahana (Fig. 3.4), a field of hot springs and fumaroles underlain by the same geothermal system that feeds the modern Waimangu field (e.g. Nairn 1979). At 3:20 a.m. a severe earthquake occurred, probably marking the time when the active geothermal system at Rotomahana began to be disrupted violently by interaction between magma and superheated water (Houghton and Wilson 1998). Activity then continued along the entire 17-km length of the eruption fissure until 6:00 a.m. (Williams 1887). In contrast with eruptions at Mt Tarawera, the explosions at Rotomahana generated both a high liquid-water-rich plume and turbulent pyroclastic density currents composed of blocks, ash, and steam, which destroyed four villages (Nairn 1979). Accumulation of fine damp ash on rooftops caused building collapses that accounted for most of the 108 known deaths (Keam 1988).

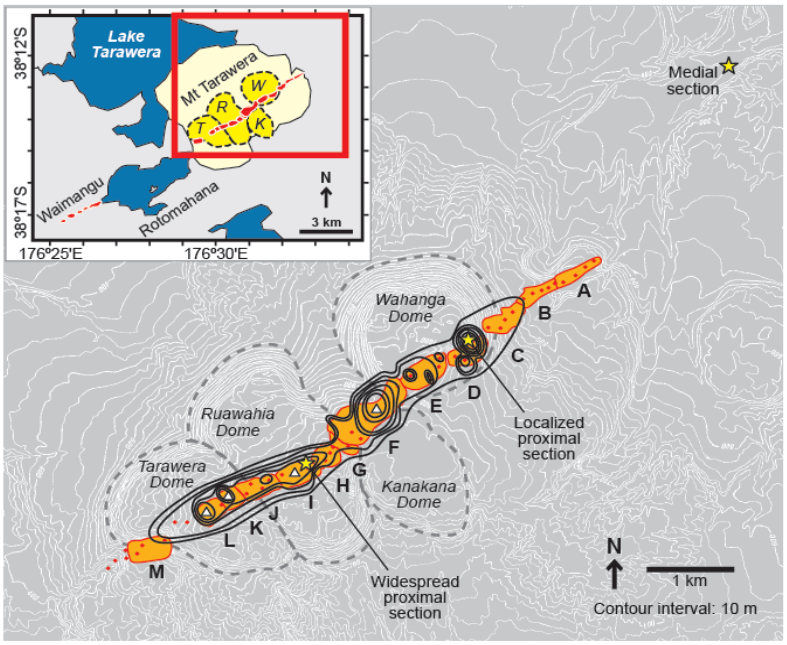

Figure 3.5: Topographic map of the Mt Tarawera area (enclosed in rectangle on inset map) with isopachs showing thickness of unit 2/3 of the 1886 proximal deposits (10 m contour interval). Main rhyolitic domes of the Mt Tarawera dome complex are marked with dashed outlines and labeled in italics (abbreviated W, R, K, T on inset map). Capital letters label the thirteen craters along the 8 km long Mt Tarawera fissure segment. Triangles mark locations of the four likely sources of Plinian plumes (from Sable et al., 2006). Stars mark the three key sections: widespread proximal, localized proximal, and medial.

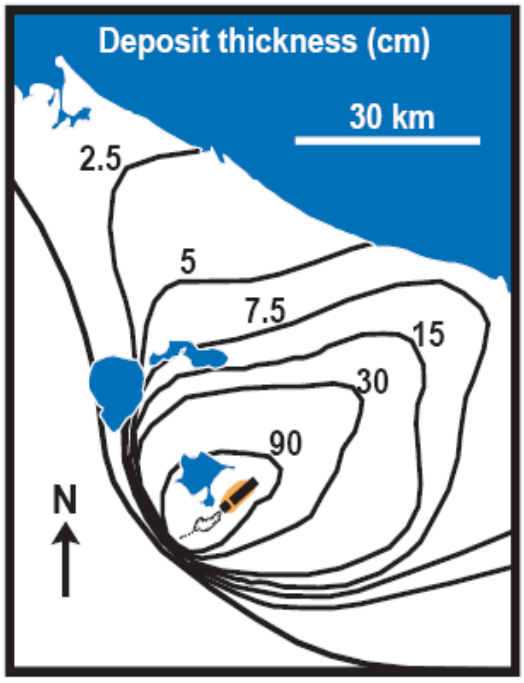

Figure 3.6: Isopach map of widespread scoria fall from the Tarawera 1886 eruption, after Walker et al. (1984).

Widespread deposits

The southwestern portion (Rotomahana-Waimangu) of the 1886 eruptive fissure (Fig. 3.4) was the source for the fine-ash-rich deposits with common accretionary lapilli collectively called the Rotomahana Mud (Nairn 1979). The southwestern deposits include localized pyroclastic density current deposits and a widespread fine-ash fall with a northerly dispersal that forms a significant component within the upper levels of the otherwise scoria-dominated 1886 fall deposits.

The northeastern vents produced both sheet-forming and cone-building deposits of basaltic scoriaceous lapilli (Walker et al. 1984). The widespread scoria sheet covers an area of 6000 km^2 within the 2.5 cm isopach (Fig. 3.6), and an estimated total area of 10,000 km^2, with a dispersal axis toward the northeast (Thomas 1888; Walker et al. 1984). The large extent and low rate of thinning (bt = 4.3 km after Pyle 1989) qualify the deposit as Plinian, with an estimated column height of ~28 km (Walker et al. 1984). Median grain size of the widespread scoria fall decreases systematically with increasing distance, changing from -3.3 ϕ (1 cm) at 1 km to 2.3 ϕ (0.2 mm) at 40 km from vent; however, these values include up to 15% of the fine-grained Rotomahana Mud (Walker et al. 1984).

Proximal deposits

The cone-forming proximal deposits surround the 7-km-long Mt Tarawera portion of the rift and are confined to an area within 400 m of it. The northeastern proximal 1886 deposits consist of a series of truncated, partially overlapping scoria cones, or more accurately half-cones (Fig. 3.7). The deposits are well exposed and consist of a series of moderately to well-sorted lapilli-and-bomb beds with a total thickness between 35 and 75 meters along the fissure. Most of the beds dip outwards away from the fissure and show rapid changes in thickness both parallel and perpendicular to the 1886 fissure (Sable et al. 2006).

The simplification of the stratigraphic units introduced by Walker et al. (1984), used here is: phreatomagmatic unit 1; dominantly magmatic unit 2/3; phreatomagmatic unit 4/5. Each of

these three units can be traced and correlated along the walls of the 8 km northeastern fissure segment. The units are as follows:
(1) Unit 1, a black, phreatomagmatic scoria-fall deposit with moderately vesicular and sometimes quenched basaltic clasts, together with subordinate rhyolite wall-rock fragments erupted during phase I of the eruption.
(2) Unit 2/3, a bedded red and black scoria fall deposit with variable but generally low contents of rhyolitic wall-rock lithic clasts. The unit forms alternating welded and non-welded subunits that thicken and thin along the rift. We interpret this unit as the proximal equivalent, in time (phase II), of the widespread fall deposit.
(3) Unit 4/5, a white, phreatomagmatic lapilli-and-block rich unit dominated by rhyolite lithic fragments with subordinate dense quenched basaltic clasts, and sparse amounts of "Rotomahana Mud" (Nairn 1979), formed at the close of the eruption (phase III).

Houghton and Wilson (1998) presented field evidence that the widespread Plinian fall deposits largely accumulated during phase II, simultaneously with the proximal unit 2/3, rather than representing only the later stages of unit 2/3 accumulation (cf. Walker et al. 1984). However, along the fissure, the sequence of beds making up unit 2/3 varies greatly at different locations, in ways that are not immediately compatible with deposition from a classical Plinian plume (Sable et al. 2006). These lateral changes are primarily expressed in: (1) dispersal characteristics, with high variations of thinning rates of beds in crater walls parallel to the fissure; (2) variations in juvenile clast properties, i.e. grain size, vesicularity/density and morphology; and (3) content of wall-rock lithic clasts. A complication in interpreting proximal transport and deposition of pyroclasts is that all beds must also contain a mixture of clasts erupted from different point sources along the ca. 8 km long segment of the fissure (Sable et al. 2006).

Packages
Sable et al. (2006) have grouped beds of like character within proximal unit 2/3 into "packages", each consisting of several beds of similar dispersal (e.g., Fig 3.8, Fig 3.9). They recognized that at any one site, as well as between sites, packages can vary considerably in terms of dispersal, as reflected in thinning half distances. Some packages are characterized by smaller scale fluctuations in grain size and especially lithic clast content defining bedding on a meter scale whereas other packages are relatively uniform throughout. Many beds contain a juvenile population of highly vesicular, ragged and fluidal scoria. Thinning half distances for these packages (typically 20 to 35 meters) reflect the most rapid lateral changes in thickness. Other packages at the same site contain a wider range of juvenile clasts from ragged scoria to denser clasts with quenched surfaces. These packages commonly have longer thinning half distances of up to 270 m.

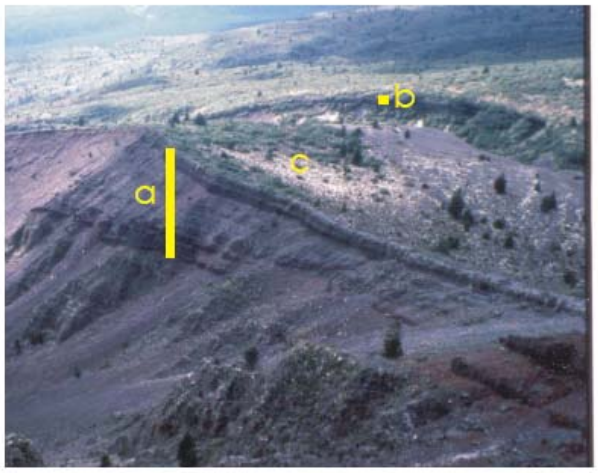

Figure 3.7: Photograph showing rapid radial thinning of the proximal deposits perpendicular to the 1886 fissure adjacent to crater D. Measured sections of the 1886 ejecta at (a) and (b) are 40 m and 2.8 m thick respectively. This rapid thinning imparts a steep primary dip to the proximal deposits. (e.g. surfaced labeled (c)).

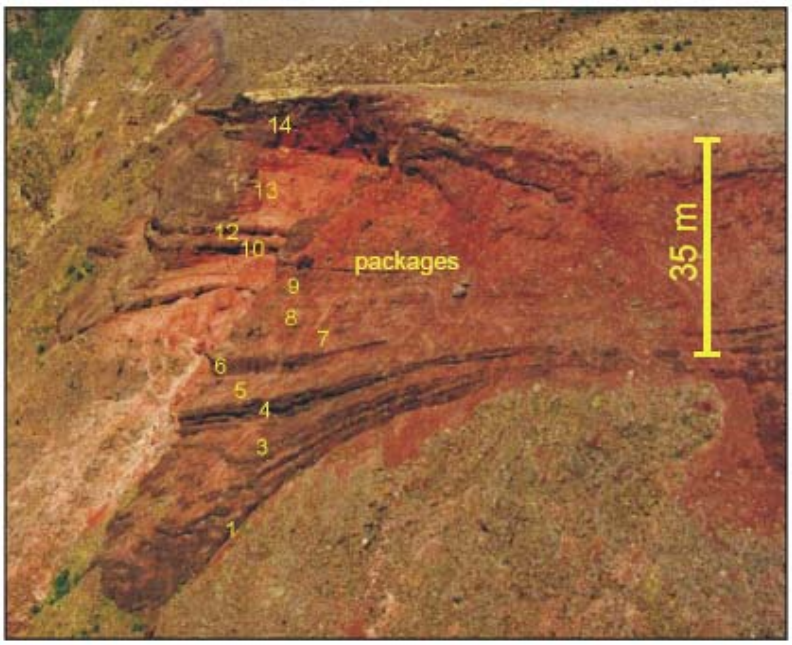

Figure 3.8: Photograph showing the distribution of packages at section T28. Note the contrasting dispersal of adjacent groups of packages.

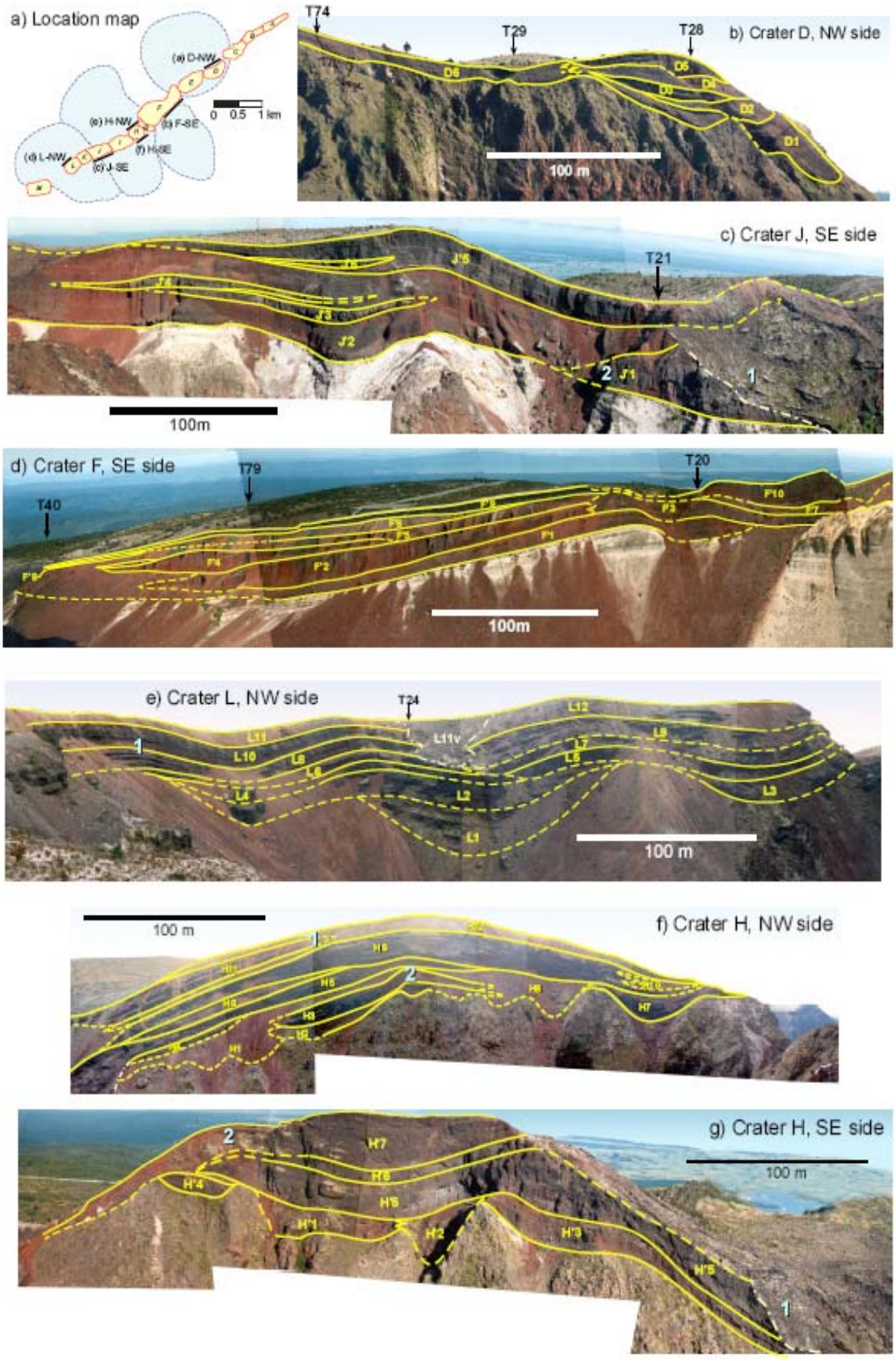

Figure 3.9: Sketches of package geometry for representative 1886 craters at Mt Tarawera. (a) Locations of lines of section; (b) northwest wall of crater D; (c) southeast wall of crater J; (d) southeast wall of crater F; (e) northwest wall of crater L; (f) northwest wall of crater H; (g) southeast wall of crater H. Locations of detailed stratigraphic sections are named and marked with arrows. Numbers refer to sites mentioned in the text. Thickness half-distance values for sections T28 and T79 are listed in Table 2.

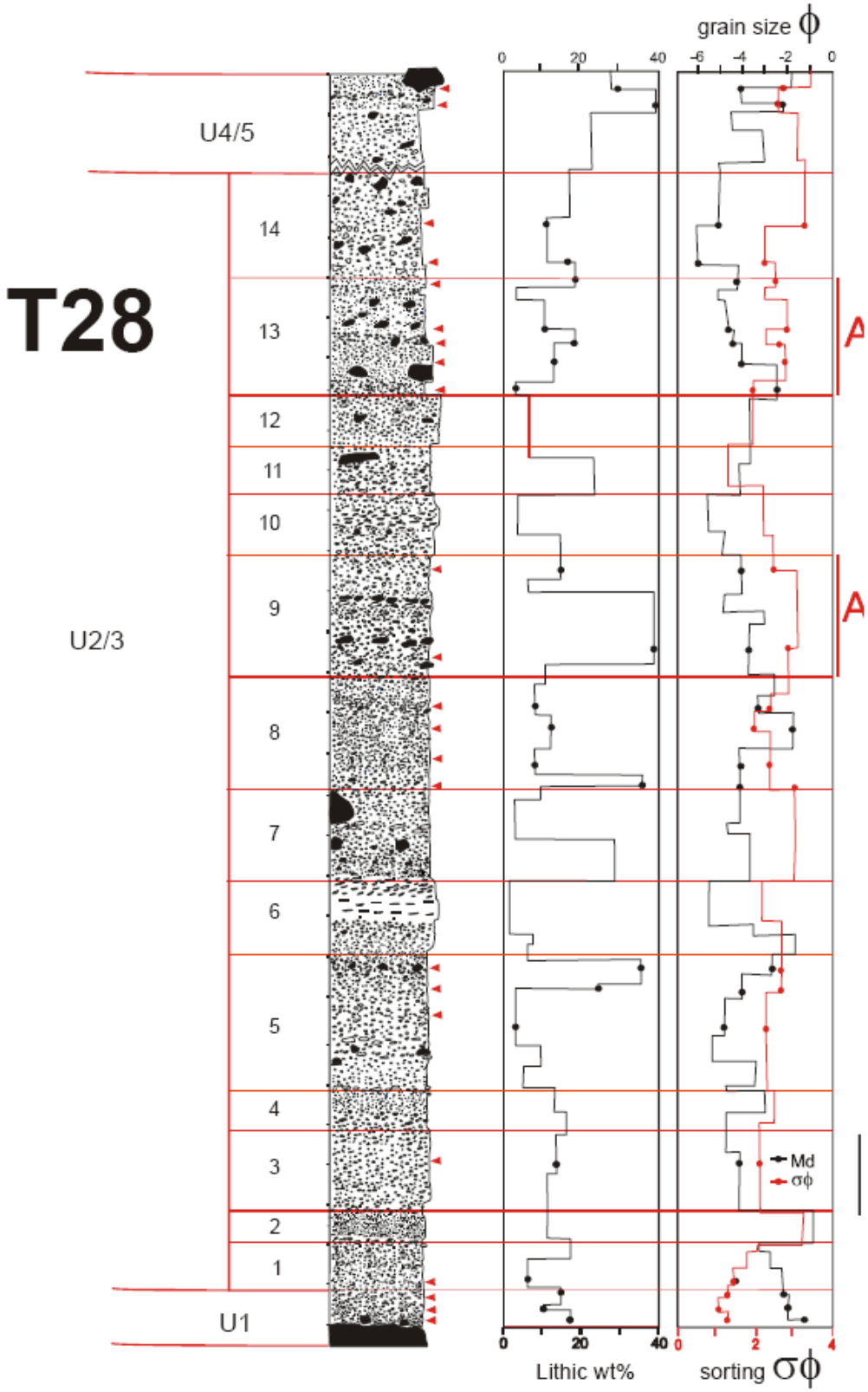

Figure 3.11: T28 stratigraphy, lithic wt%, grain size and sorting characteristics of proximal deposits. Packages that contain end member facies a beds (strongly cone forming, less widely ddispersed, with high vesicular juvenile clasts) are labeled with A.

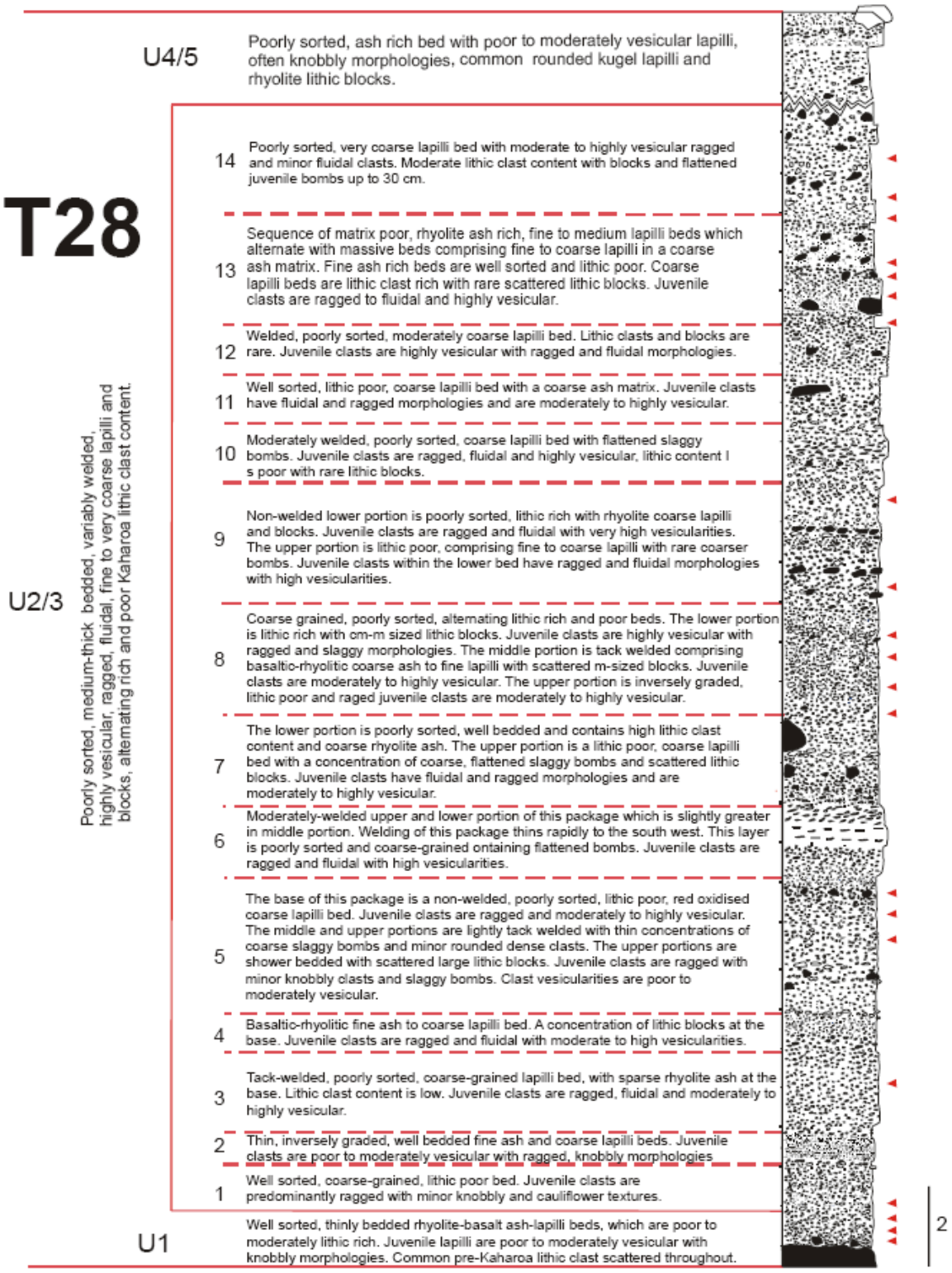

Figure 3.10: Stratigraphic section and packages descriptions for T28 proximal deposits. Open symbols are juvenile clasts, black lithics. Section height is 31 meters.

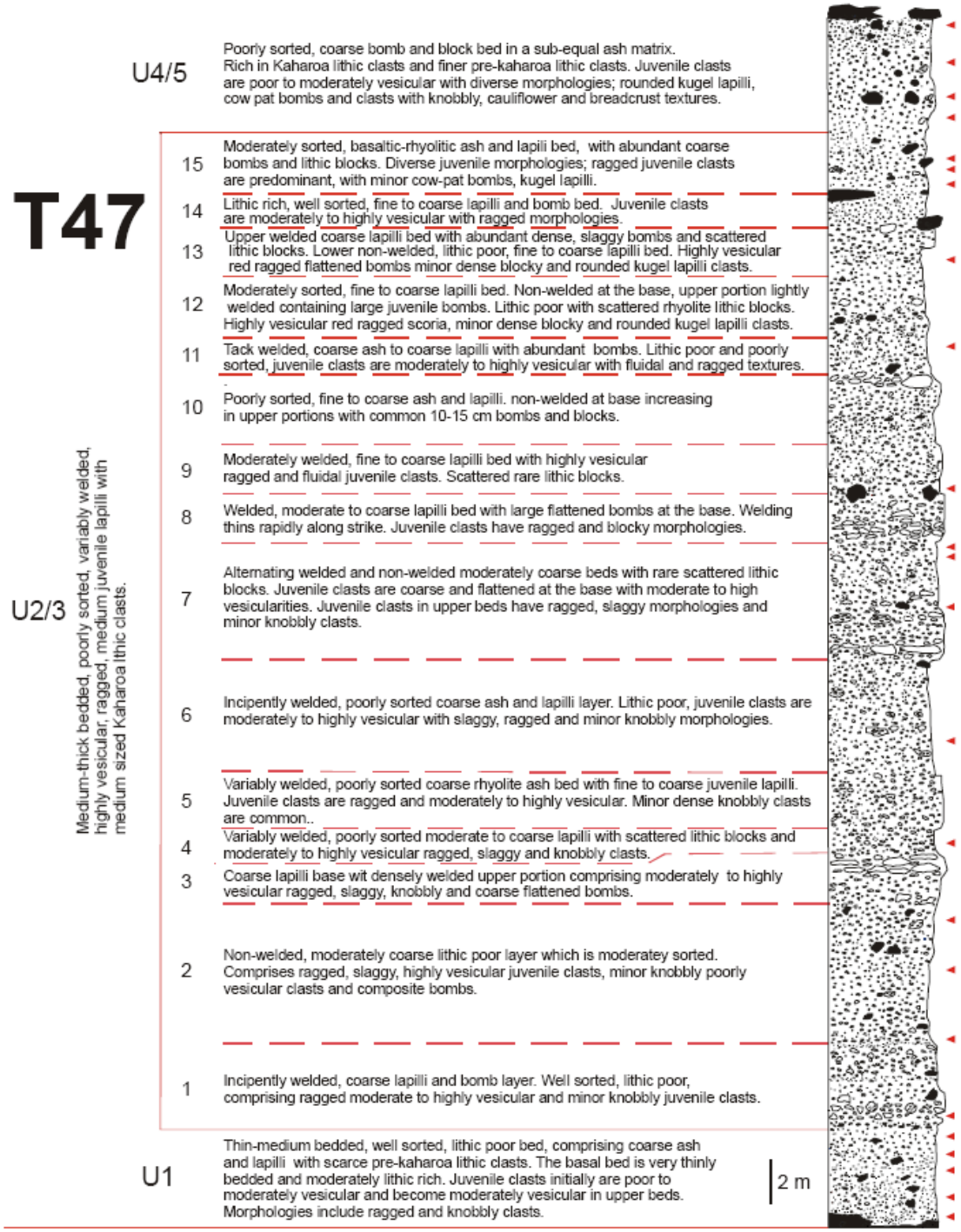

Figure 3.12: Stratigraphic section and package descriptions for T47 proximal deposits. Open symbols are juvenile clasts, black lithics. Section height is 52 meters.

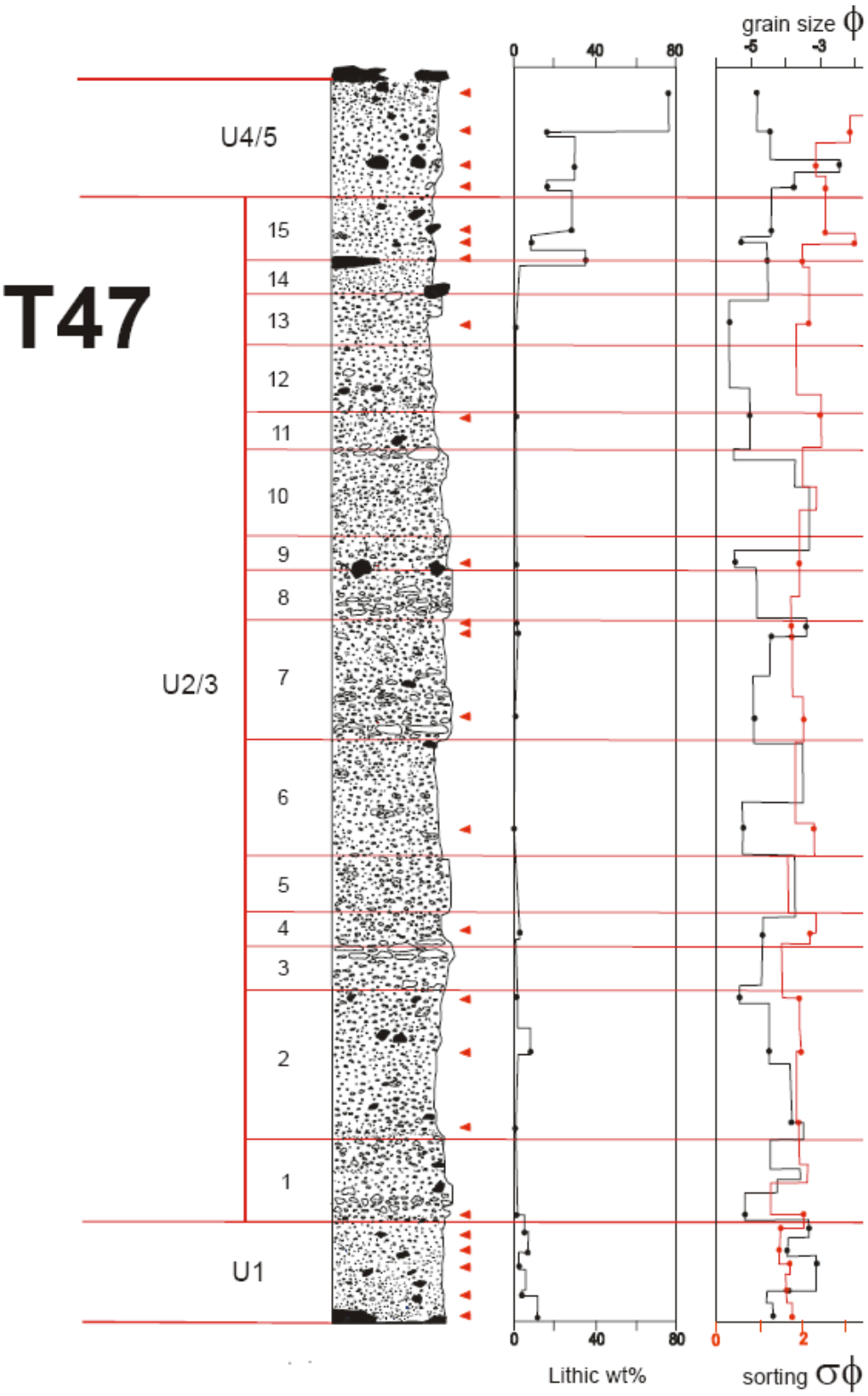

Figure 3.13: T47 stratigraphy, lithic wt%, grain size and sorting characteristics of proximal deposits. Packages that comprise end member facies b beds (less lateral thinning, more widely dispersed and lower visicularity juvenile clasts) are labeled with B.

Several craters are dominated by packages with only a narrow range of dispersals. Localized packages dominate craters D and E, and widespread packages dominate craters F, H, J, and L.

A representative section for the localized endmember is T28 on the northwestern wall of crater D (Fig. 3.8, 3.9b), where all packages are localized, with t1/2 between 20 and 35 m. This will be our main study site (Figs. 3.10, 3.11). Many beds within the packages show various degrees of agglutination, ranging from weak tack welding to moderately strong welding where clasts adhere firmly to each other but still have distinct boundaries. Clasts of glassy, coarsely re-vesiculated rhyolite are commonly found encased in basalt. Basalt clasts generally have a red oxidized color. The grain size is coarse, and sorting is moderate to poor due to the abundance of ash-sized wall-rock particles; quantitative grain size analyses are presented in Carey et al. (2007). Basalt clast morphologies are typically ragged, slaggy, and knobbly. The wall-rock lithic content is typically 5-15% and rarely up to 40%, ranging in size from ash to 20-30 cm blocks and rare 1 m blocks.

Characteristic examples of the opposite extreme are section T79 in crater F (Fig. 3.9d), and T47 in crater H (Figs. 3.12, 3.13). Packages are typically non-welded and massive to weakly bedded. The grain size ranges from coarse ash to 10-20 cm bombs, but is dominated by fine to coarse lapilli. Wall-rock lithic content is 5-20% in the form of ash and scattered blocks. Juvenile clasts are commonly red to brown, with ragged, knobbly or blocky morphologies. Some dense cauliflower bombs are present, along with a minor proportion of slaggy clasts.

Grain size, componentry, vesicularity: phreatomagmatic phases I & II
The opening and closing phreatomagmatic units 1 and 4/5 can be distinguished on the basis of both morphology and vesicularity of the juvenile clasts and the nature and abundance of the wall rock component. The basal unit 1 deposits contain a mixture of scoria and knobbly dense lapilli which changes to a more uniform population of ragged scoria in upper beds within the unit. At all sections, juvenile clasts have typically wide vesicularity ranges, between 31 and 72%, with modal vesicularities between 45 and 64%. The broad range of clast vesicularities in unit 1 implies that vesiculation was halted at different points in the degassing history of the portion of melt ejected at any one instant in time probably due to magma/water interaction deep in the conduit (>300 m depth). A change to an increasingly narrow unimodal population of highly vesicular clasts suggests that with time, the majority of the melt was rising relatively rapidly and actively vesiculating at time of fragmentation.

Wall rock lithic clasts are present throughout unit 1 in varying proportions. In particular, the abundance of pre-Kaharoa lithic clasts (from rhyolitic eruptions prior to 1314 AD) within unit 1 is greater than for following units. Pre-Kaharoa lithic clasts show a continual decrease with time and stratigraphic height. We interpret this to mean that fragmentation began at relatively deep levels (>300 m) with access of groundwater, but then rapidly became shallower as the eruption proceeded and an increase of magma flux allowed the fragmentation surface to rise to levels above the water table by the close of phase I. (Pre-Kaharoa lithic clasts are scarce to absent in unit 2/3 deposits at both sections and we infer that the fragmentation surface had risen to, and remained, above the level of the pre-Kaharoa deposits for most of this phase).

In contrast to unit 1, juvenile clasts within phreatomagmatic unit 4/5 have the largest vesicularity ranges of the entire eruption, with much lower mean values of 38-45% and often polymodal distributions. The wide ranges of observed vesicularities in part reflects recycling

of previously erupted material, but may also be partly attributed to the slowing, stalling and ultimately retreat of portions of the magma within the vent and shallow conduit. Unit 4/5 also has the highest diversity of juvenile clast morphologies amongst the 1886 deposits, including kügel lapilli and dike wall fragments, and the population of larger clasts is dominated by flattened, degassed dense bombs with breadcrust textures. The vesicularity data, in combination with this diversity of juvenile morphologies, suggests that fragmentation during phase 4/5 was due to a complex mixture of internal (vesiculation) and external (magma:water interaction) factors. The transition to unit 4/5 is inferred to be the result of lower magma supply rates and partial open-system degassing, resulting in a low efficiency of fragmentation and episodic explosions. The data suggest that during the waning stages of the eruption, magma in the conduit underwent partial open-system behavior and by the onset of phase III, this relatively degassed magma was reaching the surface at a reduced rate of ascent and, as a consequence, the fragmentation surface retreated down the conduit towards the water table. We suggest that this favored renewed magma/water interaction, reflected in the increasing abundance of poor to moderately vesicular juvenile clasts with quenched textures and rounded cauliflower morphologies. A significant subpopulation of pre-Kaharoa clasts are most abundant in the final beds, suggest that the fragmentation surface was lowered to a level where explosions were occurring within the deeper, i.e., ~ >300 m pre-Kaharoa stratigraphy.

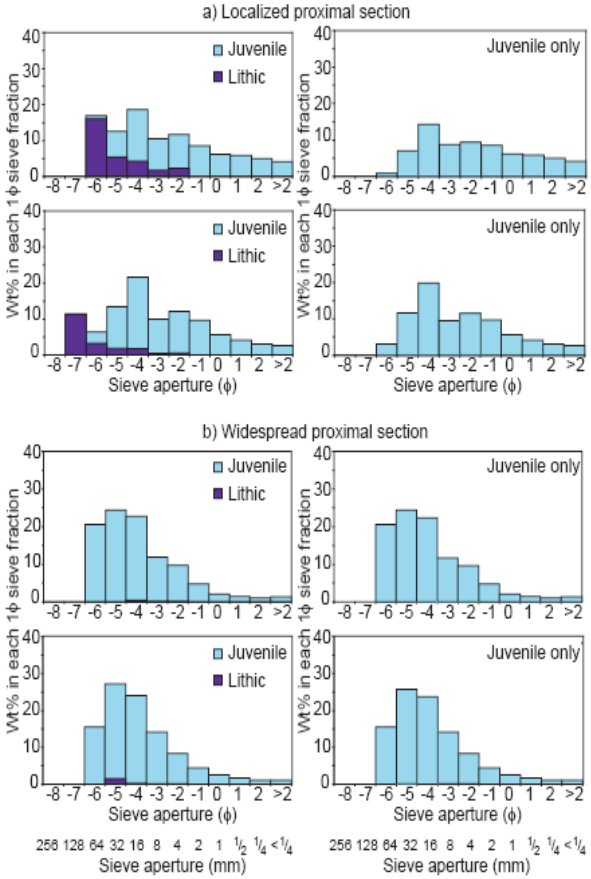

Figure 3.14: Representative grain size histograms for samples from the localized proximal section and the widespread proximal section, selected from data presented in Carey et al. (2007). The proximal localized section is richer in fines. Right column shows that the removal of the coarse lithic component from the localized proximal section's distributions improves the sorting.

Grain size and componentry: Plinian phaseII

Grain size analyses of samples taken throughout this unit reveal contrasts between packages with high and low thinning half distances respectively. For example locally dispersed T28 samples tend to be distinctly less well sorted than widely dispersed T47 samples, and sorting

coefficients decrease slightly with decreasing grain size for T47 and more steeply for T28 samples. The samples from T47 are very low in wall rock lithics and show relatively simple unimodal grain size distributions, such as typically shown by sample B (Fig. 3.14). At T28, the poor sorting and coarse grain size throughout unit 2/3 partly reflects a coarse-grained lithic subpopulation (Fig. 3.14), that is two to four phi units coarser than the mean grain size of the juvenile clast subpopulation. Removal of this coarse lithic subpopulation from the clast assemblage generates a broad unimodal distribution only slightly less well sorted than the T47 samples. This decreased sorting reflects a decoupling of a slightly coarser lithic and a finer juvenile population, which cannot be explained in terms of aerodynamic equivalence and density fractionation during transport. We suggest below that the decoupling of lithic and juvenile size is a function of the former being derived from collapse of the unstable portions of the vent walls adjacent to crater D.

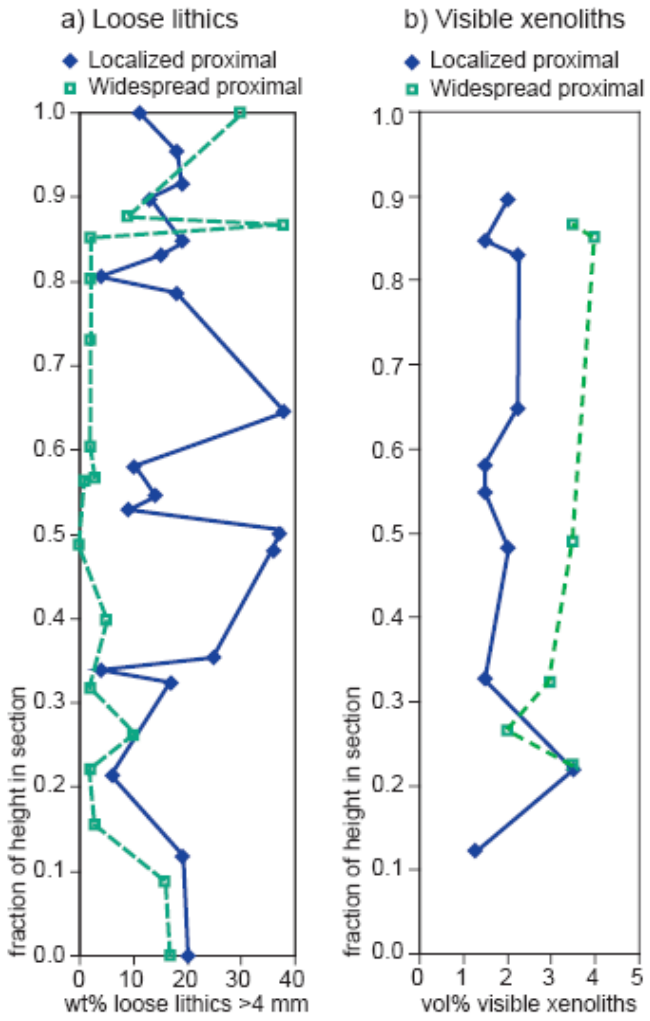

Fig. 3.15. Variation in contents of a) loose wall rock lithic fragments and b) visible xenoliths for unit 2/3 of the two proximal sections. Widespread proximal section is marked with open squares and dashed lines. Localized proximal section is marked with filled diamonds and solid lines. The localized proximal section has more loose lithics, but the widespread proximal section has a greater content of xenoliths embedded in the basaltic clasts.

Between the two sections, there is also a striking contrast in wall-rock lithic abundance in unit 2/3 (Figs 3.15). At T47, the lithic clast abundance is <8 wt% for the initial 14 sub-packages and only the last package is lithic-rich, marking a transition into unit 4/5 (Fig. 3.16). Pre-Kaharoa lithic clasts are almost absent in unit 2/3 at T47 (Fig. 3.15). In contrast, unit 2/3 deposits at T28 are characterized by a high and fluctuating wall rock lithic content (Fig. 3.16).

Alternating lithic rich and poor beds, containing identical populations of highly vesicular ragged juvenile clasts at T28, are interpreted here to reflect passive incorporation of lithic clasts accompanying instability and collapse of the vent walls.

There is a very strong link between sorting and relative abundance of wall rock lithic clasts in the unit 2/3 deposits, which we interpret to mean that the rhyolitic wall rock particles were not fragmented by explosions but have dimensions related to the joint spacing in the lavas. We suggest firstly, that the fissure crossing the outer margin of Wahanga dome adjacent to T28, has resulted in a steep and extremely fragile vent area easily accessible to failing dome material throughout phases II and III. Secondly, the fluctuations of shallow Kaharoa lithic content over short vertical intervals at T28 throughout phase II, is suggestive of episodic vent clearing following short-lived collapses that also contributed to the process of vent widening in phase III, at both T28 and T47.

How did the Tarawera 1886 magma achieve Plinian intensity?

The rarity of basaltic Plinian eruptions implies that they require an unusual set of conditions before and during fragmentation. Therefore the 1886 melt must have undergone some event atypical of basaltic systems, probably causing prolonged closed system vesiculation, leading to the acceleration necessary for Plinian eruption (Wilson et al., 1980; Woods, 1988; Papale et al., 1998).

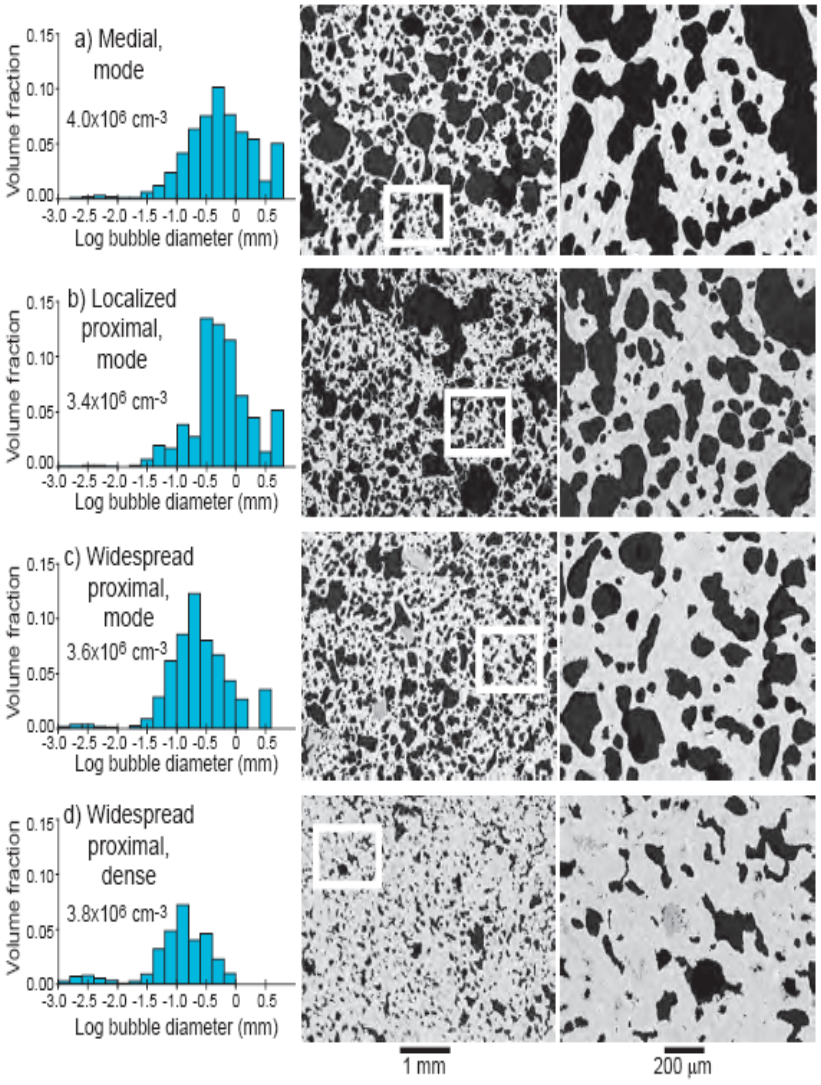

Figure 3.17: Vesicle volume histograms and SEM images where bubbles appear black. a) Modal density clast from the medial section. b) Modal density clast from the localized proximal section. c) Modal density clast from the widespread proximal section. d) Dense clast from the widespread proximal section. Modal density clasts represent the bulk of the magma in the conduit. Dense clasts show signs of outgassing.

Tarawera's bubble number densities span a limited range of relatively high values (1.5-2.5×106 cm-3; Fig. 3.17), and all the clasts have similar ranges of bubble sizes, bubble shapes, and groundmass crystallinities. This relative homogeneity indicates that all the 1886 magma shared a common early ascent history. The microlite crystallinities of the 1886 clasts are unusually high for basaltic products (e.g., Cashman and Mangan, 1995; Andronico et al., 2005; Lautze and Houghton, 2005). The high number densities of microlites and bubbles in the 1886 clasts support an interpretation that this shared early history was characterized by rates of ascent and decompression atypically high for basaltic magmas. The bubble number densities for the Tarawera 1886 clasts are 1-2 orders of magnitude higher than those observed in Strombolian and Hawaiian scoria and 1-3 orders of magnitude lower than those encountered in silicic explosive eruptions. We thus suggest that relatively high rates of ascent and decompression led to a rate of bubble nucleation that was higher than the rates in most Strombolian and Hawaiian eruptions but slightly lower than the rate in the Etna 122 BC basaltic Plinian eruption (Sable et al., 2006a).

Melt inclusions are not available in the Tarawera clasts due to the scarcity of cognate phenocrysts, but the H2O content of the 1886 magma is roughly constrained by the whole rock compositions adjusted for the presence of xenocrysts, phenocryst assemblage (plagioclase + clinopyroxene + olivine), and clinopyroxene compositions (A. Freundt, unpublished data). The normative compositions indicating an initial dissolved water content of 3-5 wt% (Moore et al., 1995). The high initial H2O content was certainly important in powering the eruption, but its influence was most likely limited to the relatively shallow conduit, because H2O typically cannot exsolve at depths of several kilometers (Wallace and Anderson, 2000). We consider the additional possibility that a high CO2 content could have played a critical role by driving some vesiculation early in ascent. We speculate that the early exsolution of significant CO2 at depth could have given an early start to the upward acceleration of the magma.

Model for variability along fissure during the Plinian phase: vent wall instability
We favor a model in which all the magma was able to vesiculate rapidly, crystallize extensively, and accelerate dramatically before fragmentation, but the emergent erupting jets were affected by differences in vent wall stability and geometry (Fig. 3.18). Carey et al. (2007) show that the abundance of loose wall rock particles in the Tarawera deposit is a poor indicator of explosivity or degree of involvement of external water but a good indicator of wall rock stability in the shallow conduit and vent. Lithic content for unit 2/3 deposits averages 2 wt% over most of the widespread proximal section, but 18 wt% at the localized proximal section. Most of these lithic particles are derived from shallow depth (less than 300m), and some are partially coated with basalt (Carey et al., 2007).

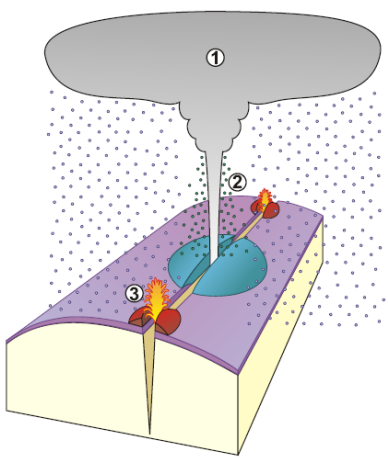

Figure 3.18: Cartoon with schematic depictions of three transport regimes. (1) Upper plume: particles are carried to the full height of the plume, travel laterally due to wind, and are showered uniformly over both proximal and distal areas. (2) Margins of jet (and lower convective plume): the relatively slow velocity and unsteady motion and particle concentration of the margins allow particles of all sizes to escape and land in the proximal area. (3) Lower-intensity explosions.

We propose that the vents that produced the localized proximal deposits had unstable walls that underwent a series of minor collapses during the 1886 eruption. Each collapse sent cold wall rock particles into the vent, where they perturbed the thermal, rheological, and dynamic properties of the ascending gas-pyroclast mixture. The temperature of the erupting jet decreased while its bulk density increased from the addition of the dense lithics. The vent wall collapse also may have led to a flared vent geometry in such locations, which could have affected the mass eruption rate and the exit velocity of the erupting gas-pyroclast mixture (Wilson et al., 1980; Woods and Bower, 1995). The geometries of the vents during the climactic phase are poorly constrained because late-stage collapses has substantially widened the craters, and destroyed or obscured previous structures (Nairn and Cole, 1981; Walker et al., 1984). In summary, we suggest that the incorporation of wall rock interfered with the development of a stable buoyant plume and made sustained eruption impossible at many locations along the fissure.

4. Tongariro composite volcano

Introduction

Tongariro is a young, active, andesite-dacite composite cone complex near the southern end of Taupo Volcanic Zone (TVZ). Its recent history is well established from 14 C age determinations and tephrostratigraphy (Topping 1973), and includes approximately 80 eruptions in historical times (Cole & Nairn 1975). The exposed portion of Tongariro volcanic complex has grown steadily since 273 ka but with intervals of rapid cone growth at 210-200 ka, 130-70 ka, and 15 ka to the present day. There is no orderly progression in space for cone-building events; the locus of activity shifted non-systematically over the lifetime of the complex within a 13 km-long and 5 km-wide vent corridor, and cone-building at some vents overlapped in time. Cone growth has varied from short-lived (<10 ky) and rapid (c.1 km3/ky) episodes, to cones where activity lasted for periods of about 50 ky at eruptive rates of less than 0.1 km^3/ky.

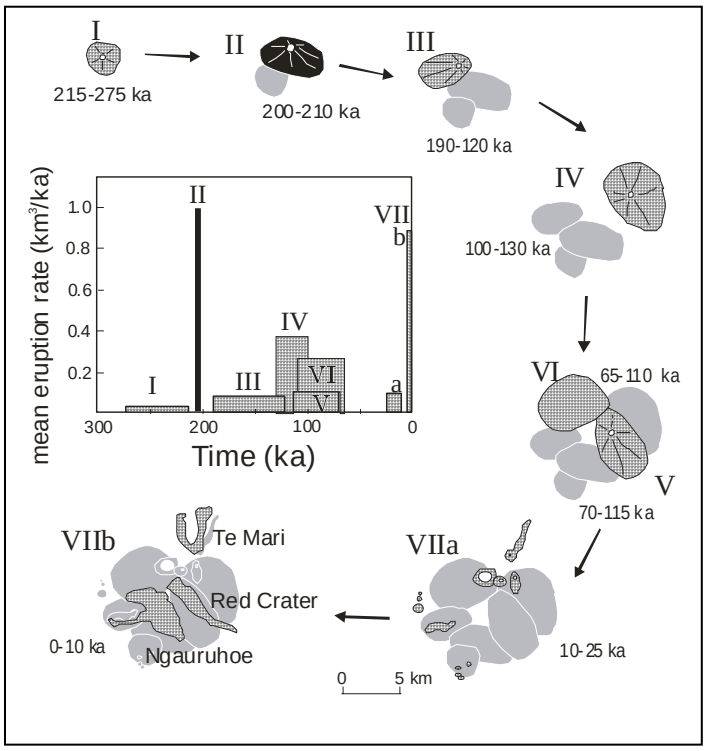

Figure 4.1: Growth of individual cones at Tongariro. Inset shows time-averaged eruption rates.

Growth of the visible portion of the complex had begun by the time interval 250-270 ka. Lavas of this age are exposed at a number of sites, but are generally isolated and surrounded by younger cone-forming sequences, so that the precise form of the early volcanic complex is unclear. The first significant cone-forming episode (Tama 1) took place between 266 and 273 ka, from a source at the southern end of complex. A major eruptive episode (Tama 2) followed between 210 and 200 ka, and a major cone formed over much of southern Tongariro with the related central vent somewhere south of the modern summit of Ngauruhoe.

The next group of major cone-building episodes took place between 180 and 80 ka. Over 30 lava flows were extruded, together with the formation of flank scoria cones at northeastern Tongariro (northeastern Oturere cone), principally in the time interval 130-100 ka. The central vent active at this time lay to the west and has been removed by subsequent erosion, but several flank vents are exposed in the northeastern wall of Oturere valley. During this time another major cone (Pukeaikiore) grew in the west from a centre in the area now occupied by the Mangatepopo valley. The pre-Holocene lavas of Pukekaikiore are the remnant of this succession.

Growth of the two further cones followed (SW Oturere and Tongariro Trig) followed between 110 and 70 ka, from central vents at southeastern Oturere and in the vicinity of Tongariro Trig. Lavas of this age covered an area equivalent to 30 % of the total composite cone.

Existing data imply a relative quiescence from 70 ka until establishment of the relatively complex system of recent vents at c. 15 ka. This interim conclusion must be tempered by an absence of data from several key areas, noticeably northeastern Tongariro, Te Mari and Mangahouhounui and by recognition of widespread erosion during the last Glacial. Recent activity began at a number of sites; Te Mari, Tama Lakes, Red Crater-Emerald Lakes, North Crater, Pukekaikiore, and Blue Lake crater (Topping 1973) but has been dominated by the rapid growth of Ngauruhoe cone since 2.5 ka.

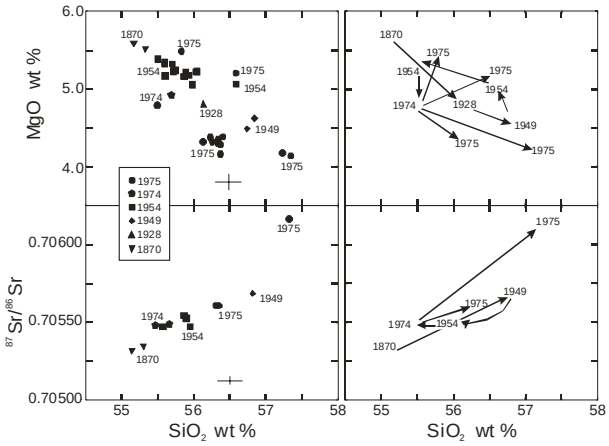

Figure 4.2: aspects of the petrology of historical lavas at Tongariro demonstrating the complex relationships between magma batches.

At Tongariro, we have combined detailed field mapping and geochronology with new geochemical analyses to examine magma evolution during short time windows of 100 (Figure 4.2) and 1000 years. This approach has provided insights into magma batches at Tongariro: they are typically small (<<0.1 km^3) and short-lived (<1 ka), and compositionally diverse. On these time scales the system is multi-process (no single geochemical trend), open (mixing of variably contaminated, isotopically diverse small magma batches), and is not unidirectional (no simple evolution with time). A scatter of data about linear or curvilinear trends suggests that multiple processes are involved, e.g. fractional crystallization punctuated by mafic recharge and magma mixing. Strong support for the involvement of magma mixing also comes from petrographic evidence such as plagioclase phenocrysts containing zones of glass inclusions (sieve texture) and strong reverse zoning, and Fe/Mg ratios of olivines and pyroxenes which are not in equilibrium with those of the host. Ion microprobe studies of

mineral phases from Ngauruhoe lavas also show complex trace element profiles consistent with a complex history of magma mixing, contamination and crystal fractionation (Rogan and Blake, 1994). Andesite is by far the most common rock type, accompanied by lesser volumes of basaltic andesite and, rarely, dacite.

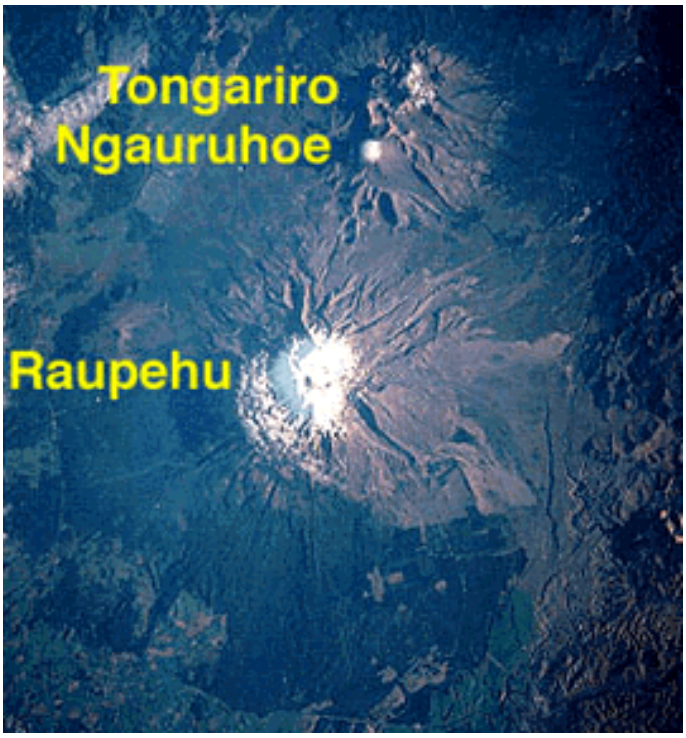

Figure 4.3. Space shuttle image of composite volcanoes in southern TVZ. Note misspelling of Ruapehu.

Figure 4.4. Panoramic view of Tongariro (right) and Ruapehu composite volcanoes.

Ngauruhoe

Ngauruhoe cone, the youngest of the Tongariro constructs, has grown rapidly over the last 2500 years in an alternation of effusive, Strombolian, Vulcanian, and subplinian eruptions of andesitic magma (Figure 4.5). At times growth has been "staccato" in fashion as evidenced in the historical record. Each historical eruption typically lasted days to months, alternating with repose periods of years to decades. Major historic eruptions occurred in 1870, 1949, 1954-56 and 1973-75 and encompassed wide variations in eruptive style. Small volcanic earthquakes beneath the volcano continue at 10 to 20 per day in late February 2007; the rate has dropped from last week. Ngauruhoe is at Alert Level 1 (some signs of volcano unrest).

Figure 4.5: A. explosive phase of the 1949 eruption (left)
B. Distribution of historical flows.

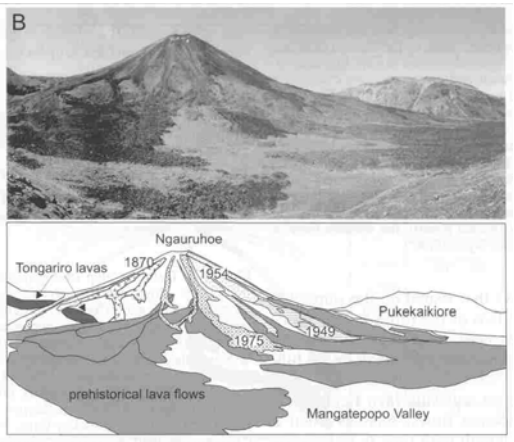

The early period of cone building appears to have been dominated by a more continuous form of activity characterized by a series of numerous frequent explosive eruptions, with associated lava flows. Eruption products preserved on and around the cone include aa and block lava flows, block-and-ash flows, ballistic blocks, a scoria cone, and tephra fall deposits. The 2.2 km3 cone has grown in a piecemeal sectorial manner reflecting constant modification to the morphology of the summit which has funneled eruption products to specific sectors on the cone.

Eruption rates can be calculated on several different timescales. Instantaneous eruption rates defined from, for example, height of eruption plumes, during the largest historical explosions were in the range 10 000 –100 000 $m^3 s^{-1}$. Discharge rates averaged over individual eruptive pulses have varied by almost two orders of magnitude (3 to 280 $m^3 s^{-1}$), reflecting variations in high level magma ascent rates and processes such as degassing. Lower rates (e.g. 0.6 $m^3 s^{-1}$) are obtained by averaging the discharge over an entire eruption lasting several months and may correspond to the magma batch(es) feeding the eruption. The long term growth rate of Ngauruhoe is 0.9 $km^3 ky^{-1}$. This is an average rate reflecting the long term deep supply rate of magma.

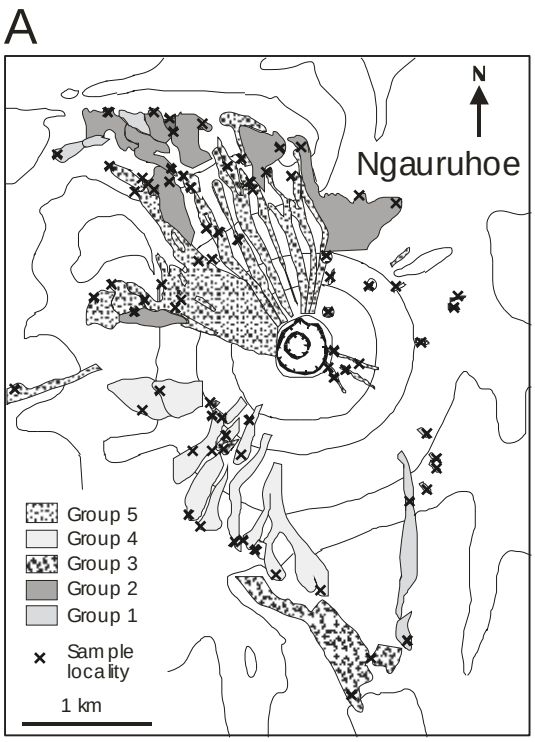

Figure 4.6. Geological map of young Ngauruhoe flows by B.J. Hobden.

The products of the 120-year historical record are principally basaltic andesite to andesite in composition, there are striking variations in composition which can be illustrated on variation diagrams such as MgO versus SiO2. There are no progressive changes in composition with time that could be ascribed to (or successfully modeled by) a single process acting on a single batch of magma, such as closed system fractional crystallization.

The complete set of Ngauruhoe products may be divided into five distinct groups on the basis of both stratigraphy and composition (Figure 4.6). The observations of geochemical variability made from the historical 100-year time window may be extended to the 1000-year window of cone activity. On the MgO-SiO_2 plot the historical samples are joined by the youngest of the prehistorical samples, which all scatter about a single broad trend (Group 5), whereas the older prehistorical Ngauruhoe lavas belong to four other distinct groups or trends (Groups 1, 2, 3 and 4) which occupy different regions both on the diagram and on the cone. Although the cone has grown rapidly, Ngauruhoe shows little evidence for the existence of large crustal magma reservoirs and long-lived magma batches. Instead, abrupt and non-systematic changes in magma chemistry and isotopic composition between and within the five groups indicate the volcano has an open system, multi-process, multi-directional character and erupts small (<0.1 km^3) and short-lived (100-10^3 yr) magma batches with no simple time-composition relationships between successive batches.

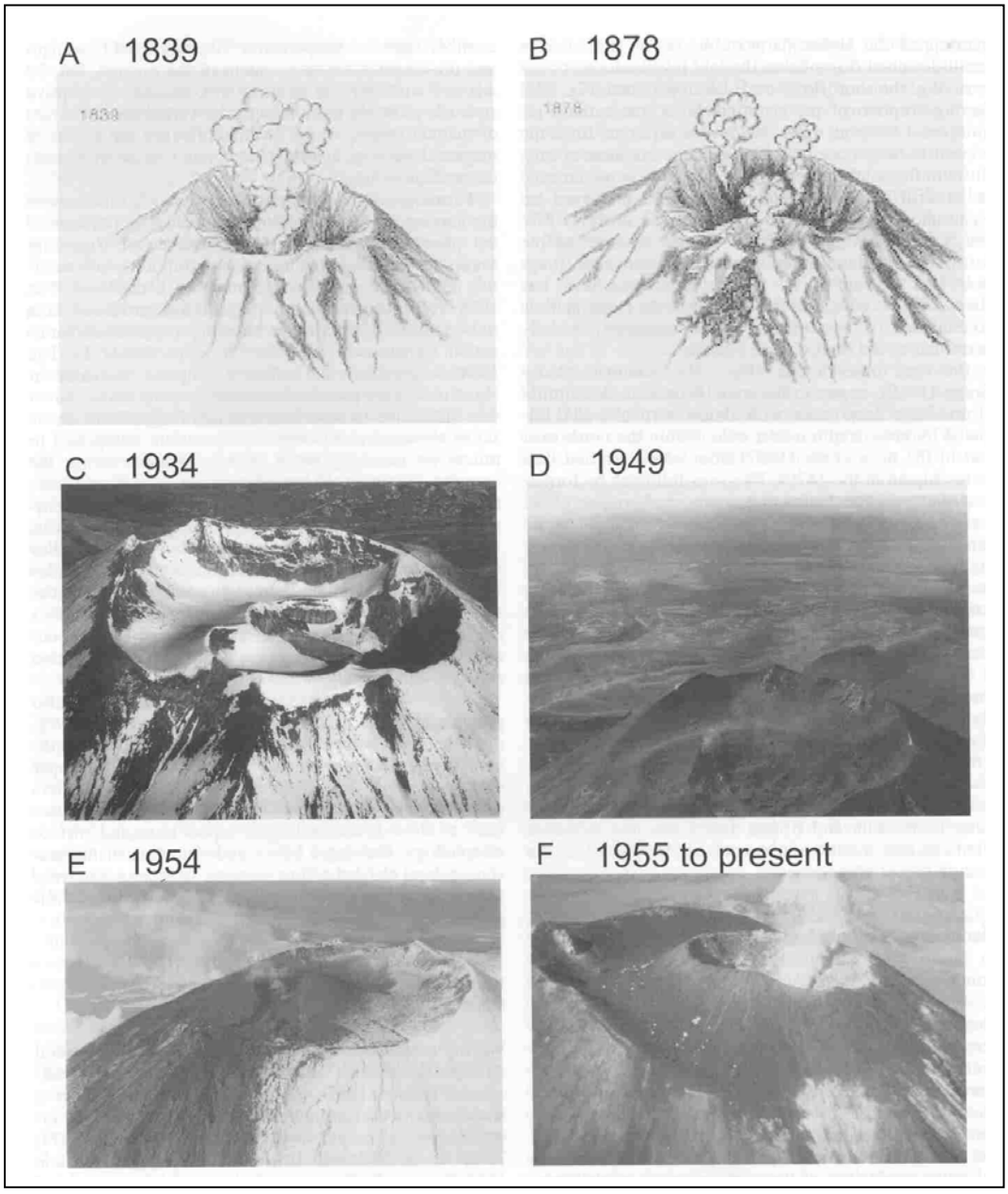

Figure 4.7: Evolution of the summit of Ngauruhoe cone. The asymmetrical development of the double cone has had a strong influence on the distribution of historical lava flow.

5. Ruapehu composite volcano

Introduction

Ruapehu is a very active andesitic composite volcano (Hackett and Houghton 1989) at the southern extremity of Taupo Volcanic Zone in New Zealand, an unusual feature of Ruapehu volcanism is the presence of a hot 400m wide acidic crater lake sitting within the active summit crater and surrounded by glacial ice.

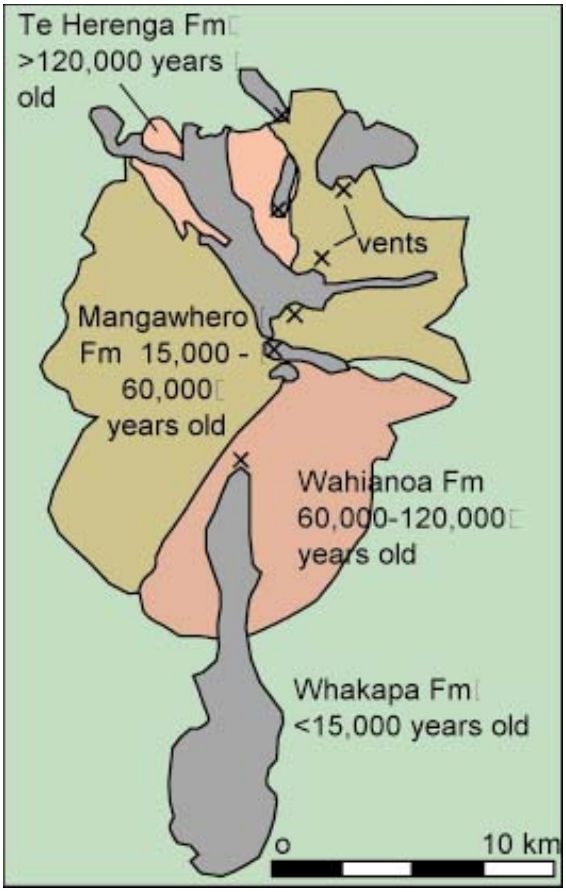

Figure 5.1: Geological map of Ruapehu *after work by W.R. Hackett.*

Ruapehu volcano was largely constructed during three major intervals of cone-growth but the products of these cones overlap to form a single large massif. First interval of cone growth was relatively uniform in composition (andesitic) and constructed a major cone that is presently exposed on the northern slopes of the volcano. This cone growth began at about 250 ka. A second cone to the east formed from 120 ka. By the time of construction of the third cone (60 ka to 15 ka) the range of chemistry had widened to include olivine basalt and dacite).

In the Holocene a series of lava fields have been constructed from summit and flank vents, a few of which extend beyond cone to the ring plain. The crater lake appears to date back to c. 2 ka. Mild explosive activity through this lake occurs essentially annually, when heating cycles culminate in small phreatic or phreatomagmatic explosions. This pattern has been broken by 18 significantly larger events in the last 2000 years (Donahue et al. 1997) each producing Strombolian or subplinian fall deposits and lahars. The volcano has been disrupted by two major sector collapses- to the north west at 9.5 ka following a period of vigorous eruption of dacitic lava and, to the east, about 4.5-3.5 ka.

Figure 5.2: Northern flank of Ruapehu volcano showing the contrasting cone and ring plain environments. Mounded topography in foreground is 9.5 ka debris avalanche deposit.

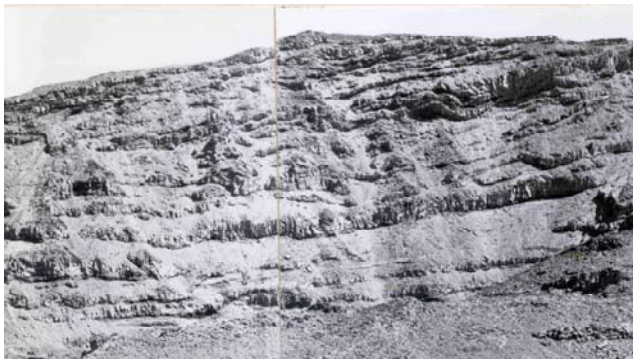

Figure 5.3. Typical cone-forming sequence through the Wahianoa Formation

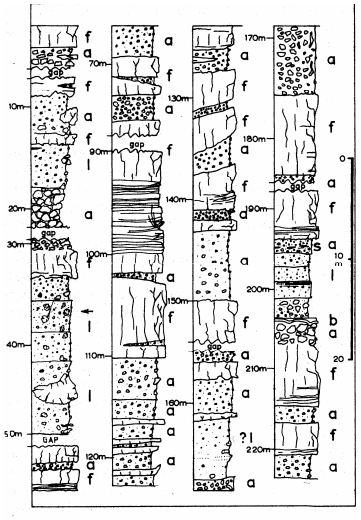

Ruapehu 1995-96

A similar episode of sporadic explosive eruptions at Ruapehu between September 1995 and November 1997 proved the most significant eruption sequence seen in New Zealand in the 20th century and second in historical times only to Tarawera 1886 in terms of impact on society. Features of the eruption were the widespread fall of subplinian ash to distances greater than 200 km from source and the large number of lahars- more than 50 in total. We can define three peaks to the 1995-97 activity, in September and October 1995 and in late June-mid July 1996, each with a different signature largely determined by magma discharge rate and factors in the shallow environment of the conduit and vent.

The lead-in to the 1995-97 eruptions was prolonged, but initially did not look any different to the near-annual heating cycles that have characterized the behavior of Ruapehu Crater Lake since 1980. The lake began to heat in November 1994; small steam explosions characterized the next summer, and a larger phreatic event on 29 June 1995 destroyed some monitoring installations. More intense explosive activity began abruptly on 18 September 1995. Numerous Surtseyan phreatomagmatic explosions occurred between 18 and 25 September, throwing ash and blocks beyond the crater and generating snow-rich lahars east and north of the vent. These early explosions ejected a very heterogeneous assemblage of vesiculated juvenile andesite bombs, lake sediments and liquid sulfur, together with lake water and steam. The liquid water precluded most of the ash-sized material from rising high into a convective plume and instead much of the particulate material was ejected in a series of spectacular vertical and inclined jets. These events typified the behavior of the volcano in September 1995 while a significant volume of water remained in Crater Lake, and liquid water was a key component of the transporting and depositing system.

A change in style in October 1995 accompanied the diminished role of the lake and a change in the discharge pattern of the andesitic magma towards more intense, prolonged eruptions. It culminated in two sustained subplinian eruptions each of which produced widespread ash fall over communities up to 300 km from Ruapehu. The first of these occurred on the night of 11-12 October and had a volume of approximately 0.02 km^3- the largest episode in 1995-6. Three days later a second shorter prolonged eruption deposited 0.01 km^3 of ash to the south-southeast.

The intensity of activity dropped markedly in late October; the last significant emission of ash in 1995 was on 18 October. Secondary lahars induced by the effect of high intensity rainstorms on the thick downwind fall deposits then became the most significant hazard, and Crater Lake became re-established (temporarily) in November 1995.
Explosive activity recommenced on 17 June 1996, two days after an abrupt return to high levels of volcanic tremor. Early weak explosions around dawn were followed by two periods of sustained subplinian eruption from 7:30 am onwards, and from 1 pm onwards. Strong wind shear displaced the columns to the northeast producing a sharply delineated weak plume (Fig. 5.4a). Other similar but smaller subplinian-sized eruptions occurred on 6-8, 10, 15 and 20 of July 1996. Alternating with the sustained eruptions in June-July 1996 were intervals of Strombolian explosions.

Activity declined sharply in late July 1996 and the eruption effectively ended with weak phreatic/hydrothermal explosions in February, October and November 1997.

17 June 1996

Following the 1995 explosions the crater lake reformed. Unrest in 1996 at Ruapehu began with the onset of weak intermittent tremor on 10 June (Sherburn and Bryan 1999). Two episodes of stronger tremor on 15-16 June 1996 were accompanied by small (Ml < 2.0) volcanotectonic earthquakes. Strong wide-band tremor recommenced at 6:00am on 17 June. At 6:50am a white thermal plume was noticed above the volcano coinciding with a sharp increase in recorded seismicity; this plume was pushed northward by the prevailing wind, while rising to an elevation of several kilometres. At 8:00am a white ash-free plume was rising to c. 500m above the volcano (3500 m elevation).

Figure 5.4: Images of 17 June 1996 Ruapehu eruption. (a) Sustained weak plume at 13:00 NZST being blown to the north east by sustained low elevation winds. (b) Moving snow-rich lahar in Whangaehu river valley on the eastern flank of Ruapehu at 8:30 NZST. Photograph T. Thordarson.

At 8:23 the first tephra-charged explosion was recorded. A black ash-rich slug rose rapidly to an elevation of 500-700 m above the crater. A series of such pulses followed at intervals of approximately one minute for a period of 10 minutes. Ash fall commenced on the northern summit plateau and off the northern flank of the volcano as the convecting mass rose to an elevation of 4-5 km (Fig. 5.4a). Curtains of ejecta periodically detached and fell from the margins of the plume, close to the crater. By 8:38, tephra-rich pulses were separated by intervals of only seconds, rising to c. 1 km above the crater and feeding a sustained convective plume blown rapidly northward. The plume was accompanied by lightening and showers of ballistic clasts.

This first phase of the eruption took place through Crater Lake and significant volumes of lake-derived water and steam entered the eruption plume. The impact of portions of this mixture of water and steam on the Whangaehu glacier generated a small snow-and-ice rich lahar on the Whangaehu glacier (Fig 5.4b).

The onset of ash fall was recorded in Taupo, at 9:31 am and Rotorua at 10:40 am, and Te Puke at 12:00 noon (Fig. 5.5). Tremor levels reached a plateau around 11:00 am and ground observers noticed a shift to a less sustained and pulsating eruption at 12:00 prior to detachment of the first plume at 13:00. Tremor levels declined rapidly at 13:30 and a series of broadband volcanic earthquakes, with coupled air waves, were recorded until 14:00. Explosive activity resumed at 14:30 with discrete explosions leading to rapid establishment of a second convective plume. This plume was also strongly affected by wind shear rising immediately to approximately 1.5 to 2 km above the vent before being displaced laterally. The intensity of the second pulse of activity had weakened dramatically by 17:00.
An interval of discrete Strombolian explosions began at 21:30 accompanied by audible detonations, volcanic earthquakes and ground-coupled airwaves (Sherburn and Bryan 1999). It had peaked by 22:00 but continued at reduced intensity for approximately 9 hours.

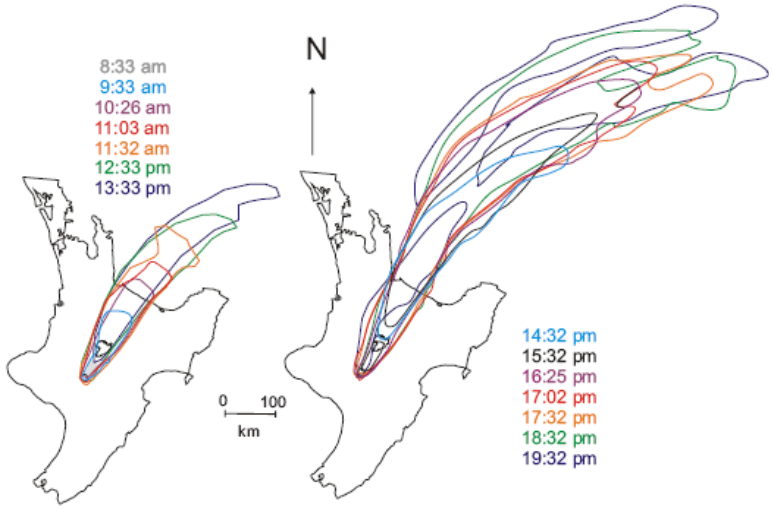

Figure 5.5: Time series of sketches of the outline of the plumes derived from JMA satellite images. Note the detachment of plume one between 12:33 and 13:33 NZST, the merger of the front of plume 2 with the tail of plume 1 by 16:25, and the bifuncation of the front of the weakened plume by 17:32.

The tephra-fall deposit from the event of the 17 June 1996 forms a narrow lobe 26-40 km wide and extending more than 200 km from the volcano, with a pronounced secondary thickness maximum about 150 km downwind (Fig. 5.6). The deposit is characterised by a sharp thickness/isomass decrease with distance in proximal areas (Fig. 5.7), varying from about 3000 kg m^2 or about 2.4 m (a few hundreds metres from the vent) to about 500 kg m^2 or 0.4 m in less than 5 km (Figs. 5.6b,c).

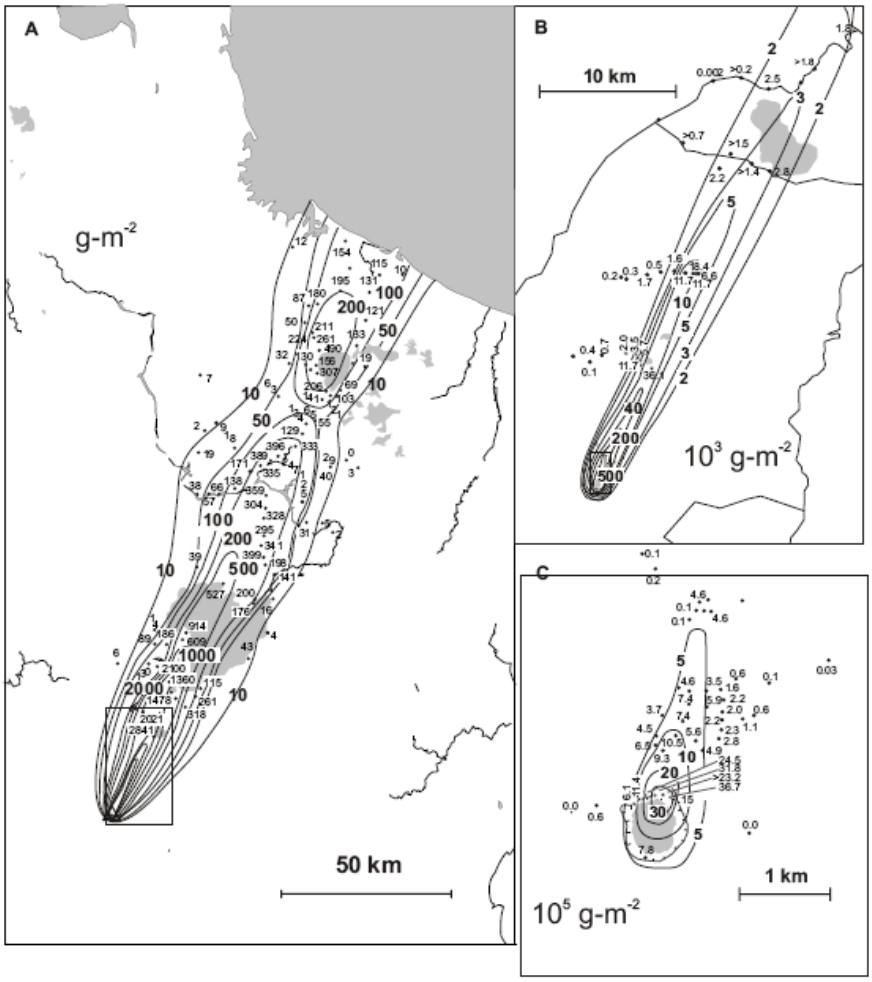

Figure 5.6: Isomass maps for complete deposit.

Close observations of proximal tephra accumulation were limited to the helicopter flight between 8:30 and 9:00 am. Three processes of tephra fall were observed all operating within 1 km of the crater rim: (1) ballistic blocks and bombs, (2) discontinuous dense curtains of tephra that detached rapidly from the rising jets, and (3) more regular and sustained deposition of lapilli and ash from the margins of the convecting part of the plumes.
Some of the best observations of distal fallout processes were made during the passage of the first plume at the Wairakei Research Centre, 120 km downwind from Ruapehu, to the east of the dispersal axis. Through the period of tephra accumulation sampling bins were placed out at 30 minute intervals. Tephra at Wairakei mainly fell as millimetric dry aggregates, similar to those ones observed during the 18 May 1980 eruption of Mount St. Helens and described by Sorem (1982). Individual clusters disaggregated immediately to form small conical piles of discrete ash particles, that merged eventually to form a somewhat discontinuous thin sheet of tephra.

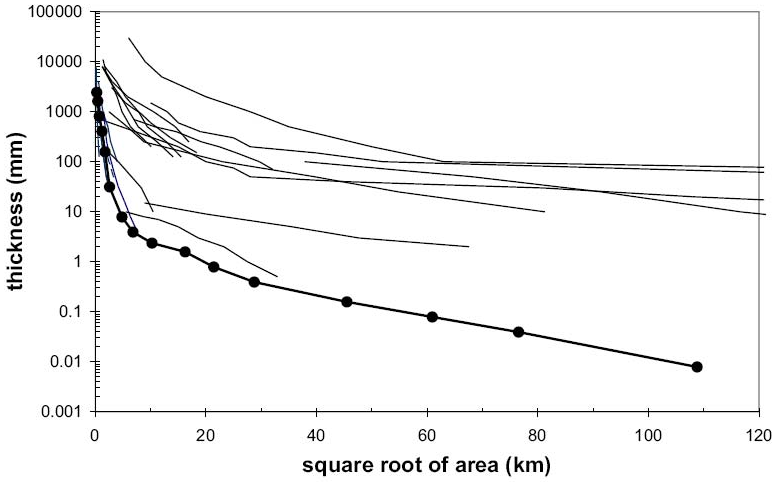

Figure 5.7: Thickness-area$^{1/2}$ plot of deposit and comparison to other eruptions.

Stratigraphically the 17 June 1996 deposits can be subdivided into 3 regions. In the distal region, beyond 30 km down wind from vent, the deposit is always a single homogeneous ash layer. Between 3 and 30 km downwind from source, in the medial region, the deposit consists of two beds, which we correlate with each of the major pulses of sustained eruption. In the proximal region (< 3 km from vent) the deposits consists of several beds with a clear distinction between two sets of beds that correspond to the products of the first and second plumes respectively (Fig. 5.8). The most proximal sections (< 1 km from vent) show some evidence for a more complex pattern of changing eruption intensity and style than can be inferred from the direct observations of the plumes.

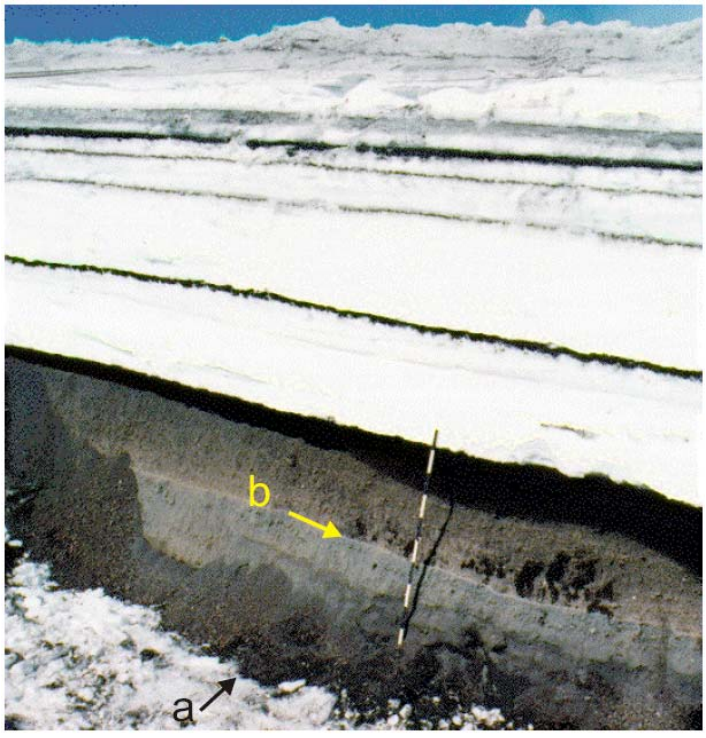

Figure 5.8: Photograph of proximal stratigraphy in 13-08-96 snow-cat pit.

The most striking feature of the proximal stratigraphy is a marked reduction in the number of recognizable beds passing outwards from vent. Note because of the uncertainty of vent position within the Crater Lake basin all distances are quoted relative to the closest point on the rim of the basin. At most proximal sites the phase 2 deposits form a single relatively uniform lapilli bed (Fig. 5.8) with weak inverse to normal grading. In contrast, in very proximal environments, i.e. on the crater rim this unit (predictably) coarsens but also overlies

two thin finer-grained fall units. We interpret the latter as the products of the weak intermittent start to phase 2, which were of insufficient dispersal to reach more distal sites. The main phase 2 bed is relatively well-sorted and rich in ragged juvenile scoria.

The contact between the deposits of phases 1 and 2 always marked by several centimetres of light grey, very poorly sorted very fine to coarse ash (marked by arrow b in Fig. 5.8), inferred to have accumulated at the close of plume 1.
The deposits of phase 1 are significantly more complex than their phase 1 analogs, at all proximal sites. At most sites several poorly sorted ash-lapilli falls are overlain by a coarse but relatively poorly sorted lapilli-block bed noticeably rich in wall-rock lithics than the phase 2 deposits. The stratigraphy on the crater rim is more complex. It begins with a fine ash-rich unit overlain by two lapilli-block beds and two lapilli falls. This part of the sequence is capped by a fine-ash-rich unit, in turn overlain by a series of coarse ash and lapilli falls and then a final lapilli-block bed.

We collected 54 grain size samples from 5 proximal pits- two on the crater rim and three in an arc to the north. Predictably for both phases 1 and 2 the crater rim samples are markedly coarser but with some overlap (Fig. 5.9). For phase 2 there is a trend of improved sorting with decreasing median grain size (Fig. 5.9) which is also observed in many other relatively dry fall deposits. The most proximal (crater rim) samples are slightly less well sorted than the northern samples, also a common feature of fall deposits where a diversity of minor proximal processes leads to a decrease in sorting values. Overall the phase 2 samples compare well with the Walker (1971) compilation of data for dry pyroclastic fall units. In contrast there is a significantly wider range and broad scatter of sorting values for Phase 1 (Fig. 5.9 (upper)), which we ascribe later to a wetter nature of the plume and ultimately of the explosions. The coarsest phase 2 units are actually relatively well sorted and most of these samples come from the lapilli-block bed at the top of this unit. Sorting is the principal contrast between the phases, as there is a largely complete

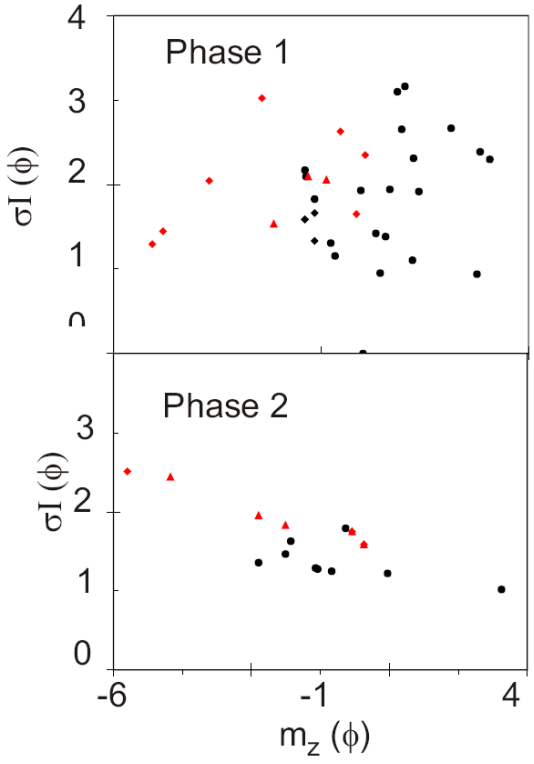

Figure 5.9: Grain size histograms along the dispersal axis.
(a) Proximal (blue) and medial (red) samples. Two distal samples (green) shown for comparison.
(b) Distal samples. Note the marked increase in fine ash content beyond 75 km down wind.

Economic consequences of 1995-1996 eruption
Three ski fields on Ruapehu were closed on 25 September 1995, with two briefly reopening for a few days in 1995. In 1996 the eruption severely limited the season. The closures resulted in the termination of several hundred jobs in the ski industry and related services. The economic losses to the local tourism industry have been estimated to be in the order of $NZ 100 million (written comm. Ruapehu District Council).

The second largest economic cost (~$NZ 21 million) resulted from damage to the hydroelectric power station and loss of production. The aviation industry reported losses in excess of $NZ 2.5 million but this figure only represents an estimate of lost revenue through cancelled flights and does not include an estimate of the economic cost to travelers of disrupted flights. The reported costs to responding government agencies included ~$NZ 5.4 million from central government, ~$NZ 454 000 from district councils and ~$NZ 205 000 from regional councils. The total cost of ~$NZ 130 million represents loss of economic production and services, damage to equipment, and expenditure on mitigation and response activities. This estimate is not the total cost, and can only represent a minimum value.

2007 lahar threat (Vern Manville, GNS)

The expulsion of Crater Lake during the 1995-96 eruption sequence, and its subsequent refilling behind a barrier of unconsolidated tephra emplaced on the stable rock sill outlet to the lake basin, has raised the spectre of a repeat of the 1953 Tangiwai lahar (fig. 5.10). The simplest worst-case scenario to simulate is failure of the tephra barrier when the lake is full to the lowest point of the dam, giving a maximum excess head of c. 7.4 m (Fig. 5. 11) and an excess lake volume of 1.6 x 106 m^3 (Keys, pers. comm.. 2005).

The fact that a Crater Lake break-out and subsequent discrete lahar event is anticipated offers an unparalleled opportunity to maximise the scientific information that could be gathered for an event of this type as well as testing predictive models.

Comparison: 1953 lahar & Tangiwai disaster
On 24 December 1953, a portion of the ice, and tephra barrier formed after the 1945 eruption and confining Crater Lake at a level higher than 1945 suddenly collapsed due to an unproven but clearly non-volcanic reason (O'Shea 1954). Approximately 1.8 million m^3 of water was released through an ice-cave as the lake was lowered by about 6 m. The waters followed the sinuous course of the Whangaehu River to the Tangiwai rail bridge 39 km downstream arriving at about 10.20 p.m. The bridge collapsed under the weight of an express train and 151 lives were lost in New Zealand's worst railway disaster (Fig. 5.12). One of the carriages was carried 2.4 km downstream and a 125 tonne pier of the bridge was shifted 64 m laterally.

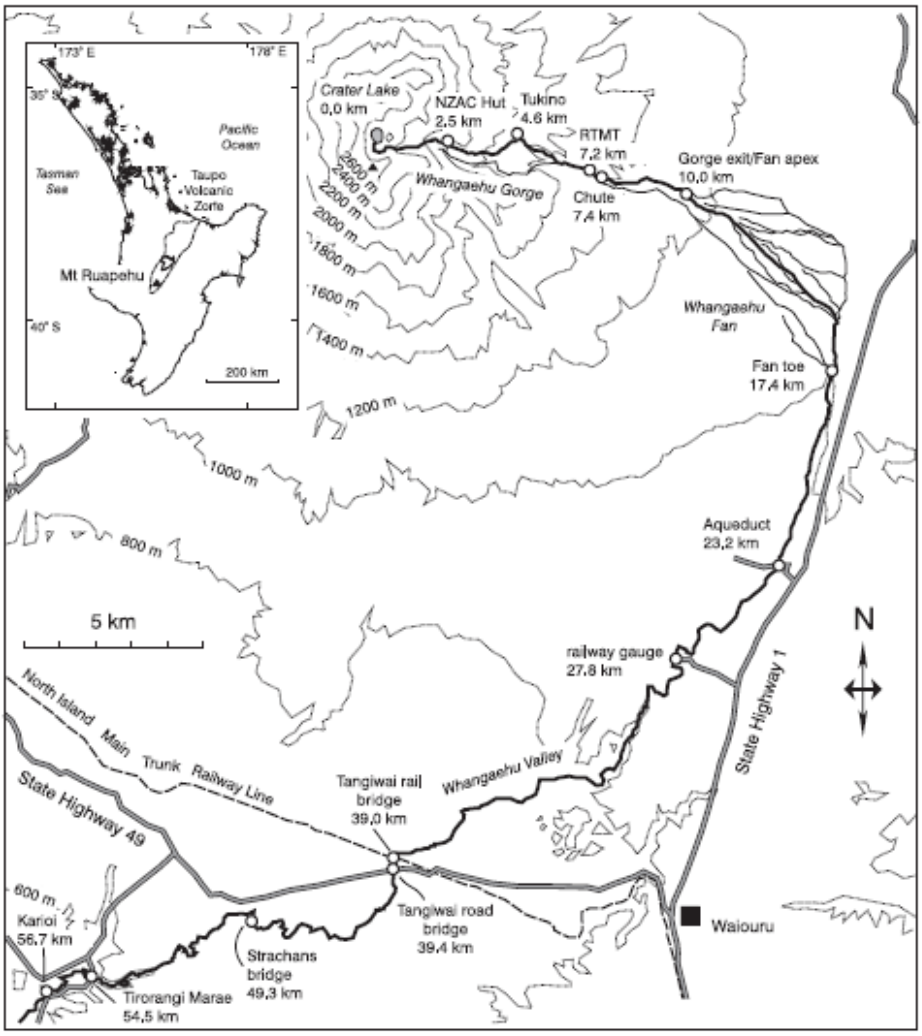

Fig. 5.10 Location map based on 1:50 000 LINZ data (Crown Copyright reserved).

Fig. 5.11 Oblique aerial view of the site of the Tangiwai Railway disaster (Tangiwai Board of Inquiry, Exhibit I 11, NZ archive).
(b) Tangiwai Railway disaster. Note displacement of bridge piers (A) and railway carriages, and coarse, bouldery nature of the lahar deposits.

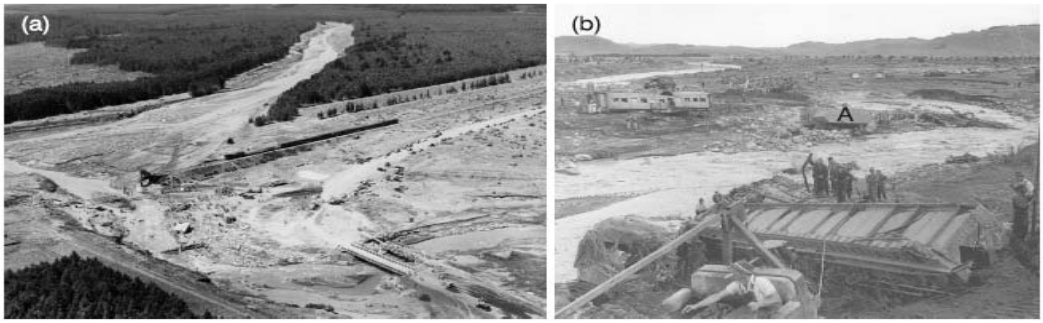

Fig. 5.12. Postulated flow paths and warning systems for a future Whangaehu lahar, from Harry Keys, Department of Conservation.

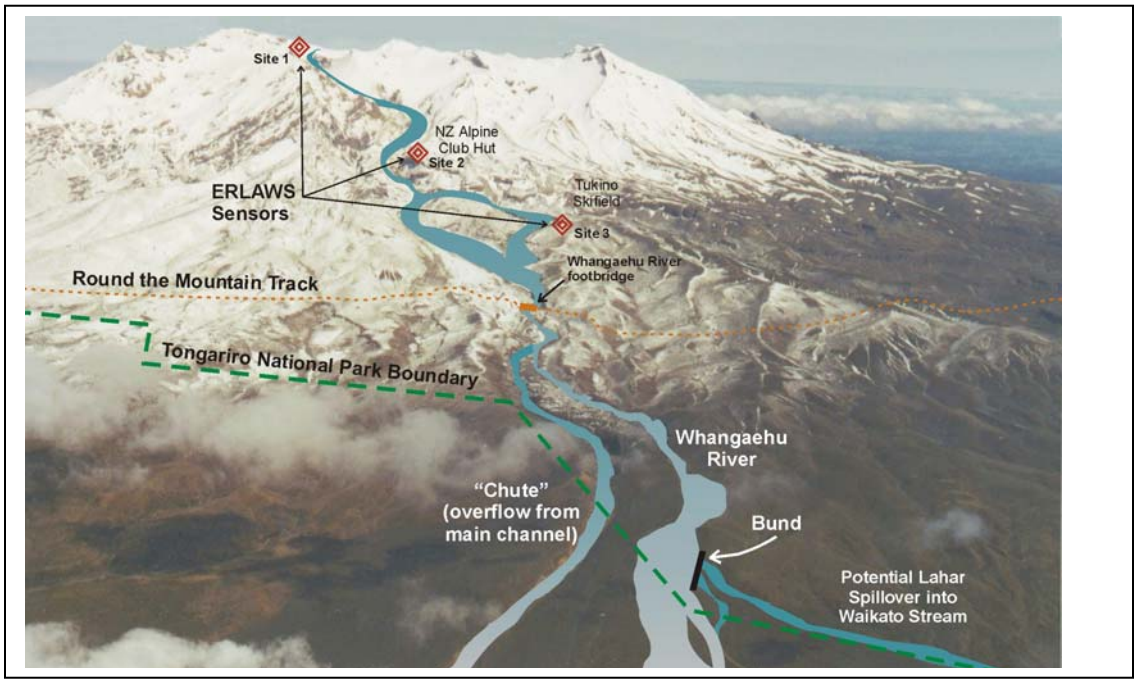

6. Taupo Volcanic Centre

Introduction

Taupo volcano (Figure 6.1) is unusual on a world scale in having experienced two young rhyolitic caldera-forming eruptions at 26.5 and 1.8 ka. Between these events, 26 other explosive and dome-building eruptions have occurred, making Taupo the world's most frequently active rhyolitic volcano (Wilson, 1993). Almost all of these eruptions took place from vents within a substantial lake (Figure 2) and many show indications of involvement of lake water in the eruptive phases. Volcanism at Taupo is now interpreted to post-date entirely the 0.33 Ma Whakamaru-group ignimbrites, and the present-day Taupo volcanic centre lies across and south of the southern margin of a larger inferred Whakamaru caldera (Wilson et al., 1986). Although age data are sparse, field data suggest that the early history (0.32 Ma to 65 ka) of Taupo is complex, involving at least 1 caldera-forming episode.

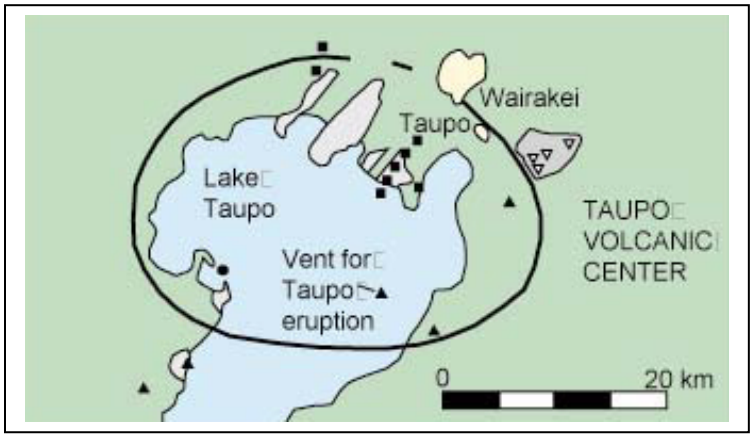

Figure 6.1 General location map for Taupo Volcanic Centre.

Figure 6.2. Taupo caldera. Tongariro and Ruapehu in background.

The 22.6 14C ka Oruanui eruption is now interpreted to be the major caldera-forming event at Taupo (e.g., Wilson, 1991). The volcano has been more frequently active since the Oruanui event than previously supposed, with evidence for 28 eruptive events (Wilson, 1993). The distribution of repose intervals and eruptive volumes suggest that the volcano may represent a chaotic system, as there is apparently no relationship between eruption volumes and the repose periods either before or after each event. Petrological studies (e.g., Sutton et al., 1994) show that many of

the Taupo rhyolites can be grouped on chemical and isotopic evidence into magma batches which shared a common source or magma body, and that sizeable batches of magma appear to have been generated and erupted rapidly, on time scales of thousands to a few tens of thousands of years. Taupo has a mean eruption rate of c. 0.2 m^3 s-1 over the past 65 ka, making it the most productive single rhyolitic volcano known.

Taupo 181 AD

The c. 35 km^3 (DRE or magma) Taupo 181AD eruption is among the most powerful explosive eruptions in the world during the past 5 ka (Wilson & Walker, 1985). Its products serve as holotypes for the most widely dispersed "dry" (ultraplinian: Walker, 1980) and "wet" fall deposits (phreatoplinian: Self & Sparks, 1978), and low-aspect-ratio (= violently emplaced) ignimbrites (Walker at al., 1980). The Taupo eruption was notable for: (i) its extreme violence and (ii) the uniform chemical composition of the magma, yet diversity of eruptive style. The eruption consisted of 7 phases (Table 6.1, Fig. 6.3), characterized by widely varying magma discharge rates and degrees of magma: water interaction, from a series of NE-SW aligned vents close to the eastern margin of Lake Taupo (Smith & Houghton 1995, Fig. 6.4).

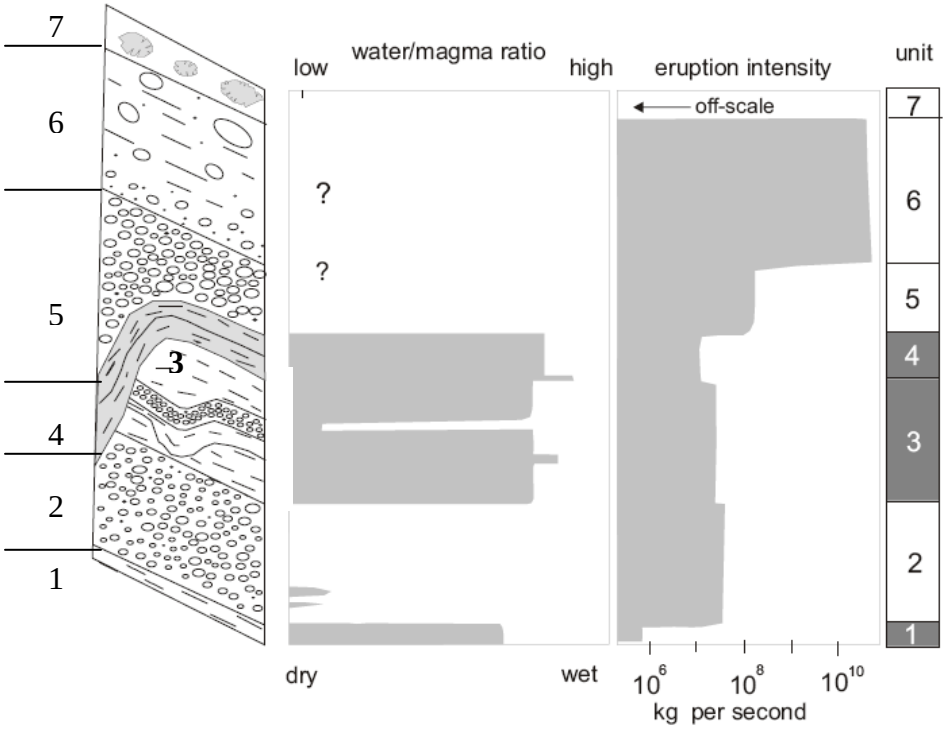

Figure 6.3. Stratigraphy and inferred eruptive conditions of the 1.81 ka Taupo eruption, modified after *Wilson and Walker* [1985]. The second and third columns are inferred relative water/magma ratios and discharge rates used by Walker and Wilson. In our current model these magma:water ratios would apply more to the eruption plume than to the fragmentation process. In the fourth column phreatomagmatic units are shown as gray.

Table 6.1: Summary of the deposits and eruptive styles during the 1.8 ka Taupo eruption, largely taken from Wilson and Walker (1985). The third column outlines the analogous stratigraphic nomenclature of Wilson (1993).

Unit this paper	Stratigraphic name	Wilson 1993	type of deposit	Notes	erupt. rate ($kg\text{-}s^{-1}$)
1	Initial ash	Y-1	Fall	weak phreatomagmatism	10^5
2	Hatepe plinian	Y-2	Fall	Moderate Plinian activity	10^7
3	Hatepe ash	Y-3	Fall	Phreatoplinian, pumiceous juvenile clasts	10^6
4	Rotongaio ash	Y-4	Fall	Phreatoplinian, dense juvenile clasts	10^5
5	Taupo plinian/early ignimbrite	Y-5	Fall+flow	Powerful Plinian and localised flow activity	10^8
6	Taupo ignimbrite	Y-6	Flow	Devastating, widespread pyroclastic density current	10^{11}
7	floating blocks	Z	Dome	Subaqueous dome growth	?

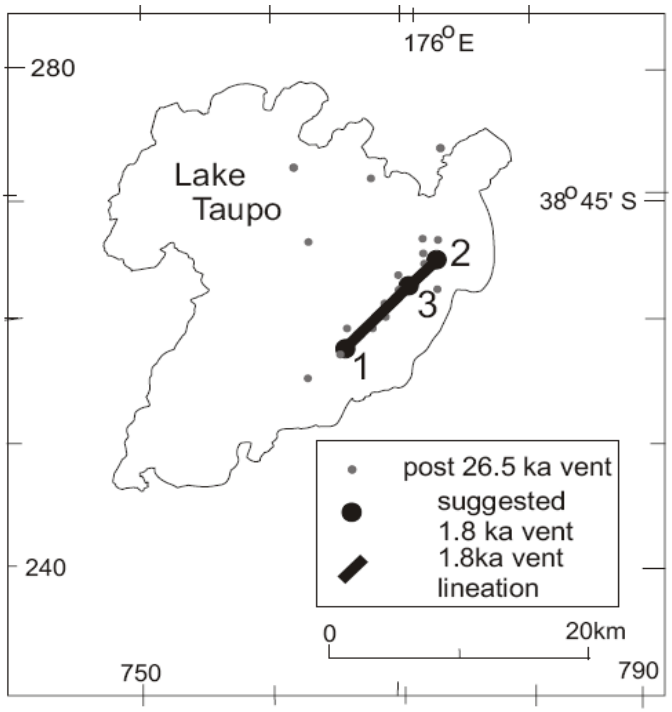

Figure 6.4. Location map showing position of post 26.5 ka vents at Taupo and the distribution of the 1.8 ka vents along a 10-km-long vent system, that is coincident with the main locus of all post 26.5 ka volcanism. After *Smith and Houghton* [1995*a*] and *Wilson* [1993]. Vent 1 was postulated as the source of Units 1 and 3 and vent 2 as the source of Unit 4 by *Smith and Houghton* [1995*a*], Vent 3 is the location of the single vent proposed for the eruption by *Walker* [180, 1981b] and *Wilson and Walker* [1985].

Eruption stratigraphy

The initial phase of the eruption was phreatomagmatic, forming a fall deposit (unit 1) exposed within 15 km of vent. Phase 2 of the eruption produced a uniform, non-graded 6-km^3 Plinian fall deposit, Unit 2 (Walker 1981a).

Units 3 and 4 are phreatoplinian fall deposits separated by a syn-eruptive erosional unconformity (Walker 1981b, Smith and Houghton 1995, Fig. 6.5). Unit 3 is dm-bedded and rich in fine ash and it is dominated by highly vesicular pumice. It contains four subunits, of which subunit 3c is a distinctive well-sorted pumice lapilli bed. Fine ash and accretionary lapilli dominate subunits 3b and 3d; the fourth (3a) contains a mixture of fine ash and lapilli. Medial and distal exposures are of fall origin; proximal outcrops contain a significant proportion of material inferred to have been laterally emplaced by 'wet', dilute pyroclastic density currents.

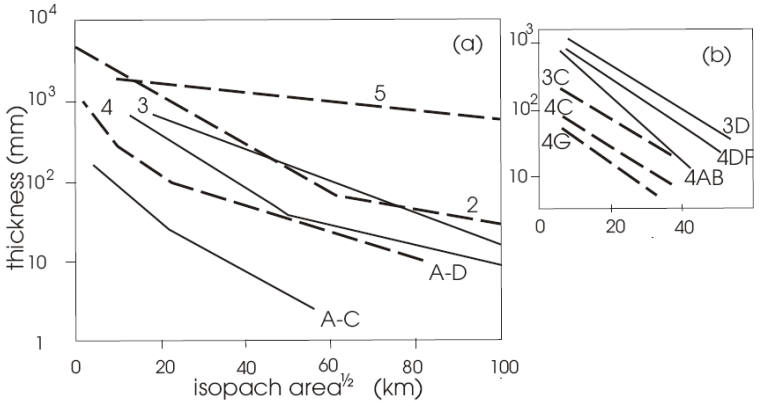

Figure 6.5: (a) A comparison of the dispersal characteristics of phreatoplinian (solid lines labeled 3 and 4) and associated plinian units (dashed lines labeled 2 and 5) at Taupo. Data from Smith and Houghton [1995a], and Walker [1980, 1981b]. For comparison data is included for the phreatoplinian (A-C) and plinian (A-D) phases of the 1875 Askja eruption, after Sparks et al. [1981]. (b) Comparable data for contrasting wetter (solid lines labeled 3D, 4DF and 4AB) and drier (dashed lines labeled 3C, 4C and 4G) subunits of the Taupo phreatoplinian units, note that wetter phases have slighter lower bt values (i.e., steeper slopes on the diagram).

Unit 4 has a similar dispersal and whole-deposit grain size characteristics to unit 3 but is very different in detail. Its key characteristics are: very wide dispersal yet exceedingly fine grainsize, with close to 100 wt% of the deposit finer than 1 mm, a finely laminated character even in the most proximal exposures, and a lack of lateral continuity over distances greater than 10 m of these fine-grained beds. Unit 4 has an extremely low wall-rock lithic content, and a predominance of grey dense juvenile clasts.

Unit 5 is the exceptionally powerful Taupo plinian deposit described by Walker (1980) as "ultraplinian', together with at least 11 pyroclastic flow units deposited by relatively weakly energetic pyroclastic density currents associated with partial collapse of the eruption plume.

Explosive volcanism culminated in generation of the highly energetic Taupo Ignimbrite (unit 6). This deposit shows many different ignimbrite facies, most noticeably a bipartite subdivision into (1) layers 1 and 2 deposits attributed to deposition from the head and body of the current, respectively (Wilson 1985).

At some stage after the close of explosive volcanism, probably an interval of between several years and a few decades, rhyolitic lava domes, whose remnants are probably represented at the present day by the Horomatangi reefs and Waitahanui bank (location 3 on Fig. 6.4), were extruded onto the floor of the re-formed Lake Taupo. Large pumiceous blocks (Unit 7) detached from the dome carapaces and floated ashore (Wilson and Walker 1985) and were incorporated in lacustrine shoreline sediments. We have sampled this material because it

provides a "window' into continued evolution of Taupo magma after the close of explosive eruption.

Juvenile clast vesicularity

The narrowest density ranges (Fig. 6.6) are present in the two Plinian deposits (units 2 and 5a). The 'ultraplinian' Unit 5 contains pumices with a lower mean density and narrower range than the plinian Unit 2, with the lowest densities found in stretched long tube pumice. Two of the three phreatomagmatic deposits (units 1 and 3) also contain mostly highly vesicular pumices but also have a "tail" of clasts of density 800 to 1100 kg m-3 equivalent to vesicularity values of 53 to 66 %. The densest clasts and widest density ranges occur in Unit 4 (the Rotongaio ash) with a density mean of 1200 kg m-3 and a range from 500 to 2100 kg m-3. The least dense clasts (density 120-300 kg m-3 vesicularity 85-95 %) occur in the two ignimbrites. The late stage floated grey pumiceous blocks are relatively dense but have a limited range of density values equivalent to vesicularities of 58 to 73%.

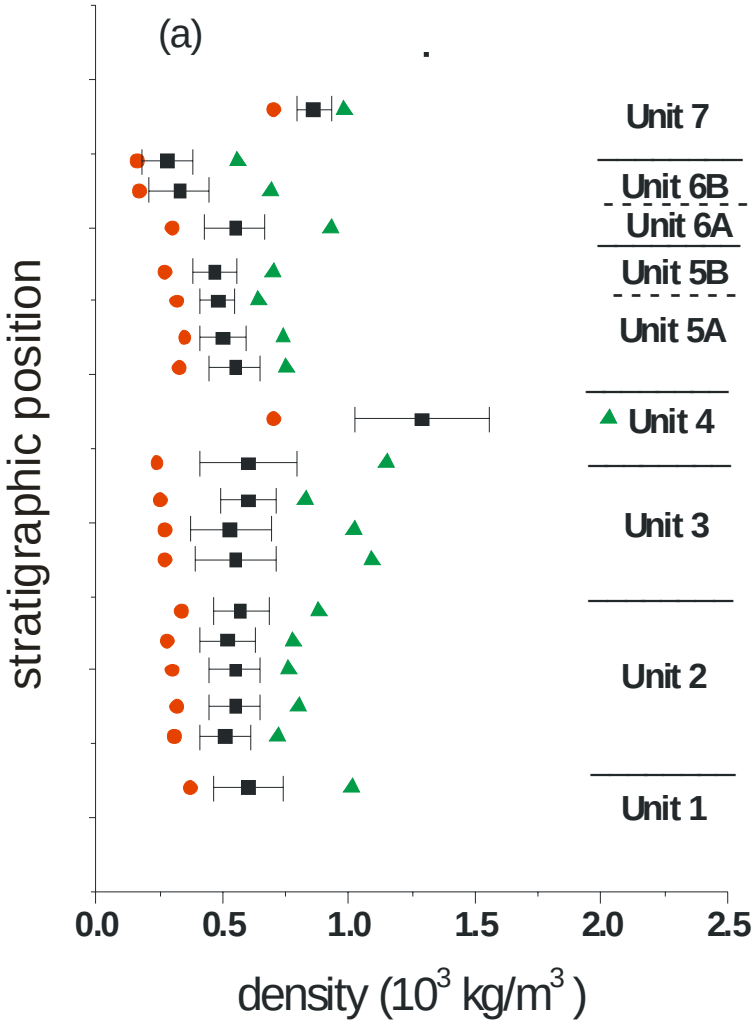

Figure 6.6. Bulk density of representative pumices from samples for the phreatomagmatic and plinian phases of the Taupo eruption. Samples consist of up to 1500 clasts. Squares are mean densities circles and triangles are minima and maxima. Note the marked contrast between the poorly to moderately vesicular clasts in Unit 4 versus the pumices that characterize all the remaining units.

TVZ general

Wilson, C.J.N. et al., 1984. Caldera volcanoes of the Taupo Volcanic Zone, New Zealand. Journal of Geophysical Research, 89(B10): 8463-8484.

Houghton, B.F. et al., 1995. Chronology and dynamics of a large silicic magmatic system: central Taupo Volcanic Zone, New Zealand. Geology, 23: 13-16.

Wilson, C.J.N. et al., 1995. Volcanic and structural evolution of Taupo Volcanic Zone, New Zealand: a review. Journal of Volcanology and Geothermal Research, 68: 1-28.

Bibby, H.M., Caldwell, T.G., Davey, F.J. and Webb, T.H., 1995. Geophysical evidence on the structure of the Taupo Volcanic Zone and its hydrothermal circulation. Journal of Volcanology and Geothermal Research, 68: 29-58.

Charlier, B. and Zellmer, G., 2000. Some remarks on U-Th mineral ages from igneous rocks with prolonged crystallisation histories. Earth and Planetary Science Letters, 183: 457- 469.

Risk, G.F., Bibby, H.M. and Caldwell, T.G., 1999. Resistivity structure of the central Taupo Volcanic Zone, New Zealand. Journal of Volcanology and Geothermal Research, 90: 163-181.

White Island

Houghton, B.F. and Nairn, I.A., 1991. the 1976-1982 Strombolian and phreatomagmatic eruptions of White Island, New Zealand:eruptive and depositional mechanisms at a 'wet' volcano. Bulletin of Volcanology, 54: 25-49.

B.F. Houghton, I.A. Nairn (Editors), 1989. New Zealand Geological Survey Bulletin. New Zealand Geological Survey, Lower Hutt, New Zealand, pp. 25-56.

Cole, J.W., Thordarson, T. and Burt, R.M., 2000. Magma origin and evolution of White Island (Whakaari) volcano, Bay of Plenty, New Zealand. Journal of Petrology, 41: 867- 895.

Hedenquist, J.W., Simmons, S.F., Giggenbach, W.F. and Eldridge, C.S., 1993. White Island, New Zealand, volcanic-hydrothermal system represents the geochemical environment of high-sulfidation Cu and Au ore deposition. Geology, 21: 731-734.

Rose, W.I., Chuan, R.L., Giggenbach, W.F., Kyle, P.R. and Symonds, R., 1986. Rates of sulfur dioxide and particle emissions from White Island volcano, New Zealand, and an estimate of the total flux of major gaseous species. Bulletin of Volcanology, 48: 181-188.

Tarawera

Cole, J.W., 1970. Structure and eruptive history of the Tarawera Volcanic Complex. New Zealand Journal of Geology and Geophysics, 13: 879-902.

Tarawera 1886 eruption

Walker, G.P.L., Self, S. and Wilson, L., 1984. Tarawera 1886, New Zealand - a basaltic plinian fissure eruption. Journal of Volcanology and Geothermal Research, 21: 61-78.

Carey, R.J.; Houghton, B.F.; Sable, J E.; Wilson, C.J.N. Contrasting grain size and componentry in complex proximal deposits of the 1886 Tarawera basaltic plinian eruption. Accepted by Bulletin of Volcanology, December 2006.

Sable, J.E.; Houghton, B.F.; Wilson, C.J.N.; Carey, R.J. 2006. Complex proximal geometry of fall deposits from the Tarawera 1886 basaltic plinian eruption: implications for eruption dynamics. Published on-line Bulletin of Volcanology. April 2006.

Nairn, I.A., 1979. Rotomahana-Waimangu eruption, 1886: Base surge and basalt magma. Journal of Geology and Geophysics, 22(3): 363-378.

Nairn, I.A. and Cole, J.W., 1981. Basalt dikes in the 1886 Tarawera rift. New Zealand Journal of Geology and Geophysics, 24: 585-592.

Rosseel, J.B.; J.D.L. White, J.D.L.; Houghton, B.F. 2006. Complex bombs of phreatomagmatic eruptions: the role of agglomeration and welding in vents of the 1886 Rotomahana eruption, Tarawera, New Zealand. Journal of Geophysical Research, 111: B12205, doi:10.1029/2005JB004073.

White, J.D.L., Houghton, B.F., Hodgson, K.A. and Wilson, C.J.N., 1997. Delayed sedimentary response to the A.D. 1886 eruption of Tarawera, New Zealand. Geology, 25: 459-462.

Kaharoa eruption

Nairn, I.A., Scutter, C., Self, S., Cole, J.W. and Leonard, G.S., 2001. Distribution, stratigraphy, and history of proximal deposits from the c. AD 1305 Kaharoa eruptive episode at Tarawera Volcano, New Zealand. New Zealand Journal of Geology and Geophysics, 44(3): 467-484.

Leonard, G.S., Self, S., Cole, J.W. and Nairn, I.A., 2002. Basalt triggering of the c. AD 1305 Kaharoa rhyolite eruption, Tarawera Volcanic Complex, New Zealand. Journal of Volcanology and Geothermal Research, 115(3-4): 461-486.

Taupo

Wilson, C.J.N., 1993. Stratigraphy, chronology, styles and dynamics of late Quaternary eruptions from Taupo volcano, New Zealand. Philosophical Transactions of Royal Society of London, A. 343: 205-306.

Sutton, A.N., Blake, S., Wilson, C.J.N. and Charlier, B.L.A., 2000. Late Quaternary evolution of a hyperactive rhyolite magmatic system: Taupo volcanic centre, New Zealand. Journal of the Geological Society, 157: 537- 552.

Wilson, C.J.N., 2001. The 26.5 ka Oruanui eruption, New Zealand: an introduction and overview. Journal of Volcanology and Geothermal Resarch, 112: 133-174.

Sutton, A.N., Blake, S. and Wilson, C.J.N., 1995. An outline geochemistry of rhyolite eruptives from Taupo volcanic centre, New Zealand. Journal of Volcanology and Geothermal Research, 68: 153-175.

Blake, S., Wilson, C.J.N., Smith, I.E.M. and Walker, G.P.L., 1992. Petrology and dynamics of the Waimihia mixed magma eruption, Taupo Volcano, New Zealand. Journal of the Geological Society, London, 149: 193-207.

Davy, B.W. and Caldwell, T.G., 1998. Gravity, magnetic and seismic surveys of the caldera complex, Lake Taupo, North Island, New Zealand. Journal of Volcanology and Geothermal Research, 81: 69-89.

Taupo 181 AD

Wilson, C.J.N. and Walker, G.P.L., 1985. The Taupo eruption, New Zealand I. General aspects. Philosophical Transactions of the Royal Society of London, A314: 199-228.

Plinian phases

Walker, G.P.L., 1980. The Taupo Pumice: product of the most powerful known (ultraplinian) eruption? Journal of Volcanology and Geothermal Research, 8: 69-94.

Walker, G.P.L., 1981b. The Waimihia and Hatepe plinian deposits from the rhyolitic Taupo volcanic centre. New Zealand Journal of Geology and Geophysics, 24: 305-324.

Smith, R.T. and Houghton, B.F., 1995a. Delayed deposition of plinian pumice during phreatoplinian volcanism: the 1800-yr-B.P. Taupo eruption, New Zealand. Journal of Volcanology and Geothermal Research, 67: 221-226.

Phreatoplinian phases

Walker, G.P.L., 1981a. Characteristics of two phreatoplinian ashes and their water-flushed origin. Journal of Volcanology and Geothermal Research, 9: 395-407.

Smith, R.T. and Houghton, B.F., 1995b. Vent migration and changing eruptive style during the 1800a Taupo eruption: new evidence from the Hatepe and Rotongaio phreatoplinian ashes. Bulletin of Volcanology, 57: 432-439.

Talbot, J.P., Self, S. and Wilson, C.J.N., 1994. Dilute gravity current and rain-flushed ash deposits in the 1.8 ka Hatepe plinian deposit, TAupo, New Zealand. Bulletin of Volcanology, 56: 538-551.

Ignimbrite

Wilson, C.J.N., 1985. The Taupo eruption, New Zealand II. The Taupo ignimbrite. Philosophical Transactions of the Royal Society of London, A314: 229-310.

Walker, G.P.L. and Wilson, C.J.N., 1983. Lateral variations in the Taupo ignimbrite. Journal of Volcanology and Geothermal Research, 18: 117-133.

Walker, G.P.L., Wilson, C.J.N. and Froggatt, P.C., 1981b. An ignimbrite veneer deposit: the trail-marker of a pyroclastic flow. Journal of Volcanology and Geothermal Research, 9: 409-421.

Wilson, C.J.N. and Walker, G.P.L., 1982. Ignimbrite depositional facies: the anatomy of a pyroclastic flow. Journal of the Geological Society, London, 139: 581-592.

Walker, G.P.L., Heming, R.F. and Wilson, C.J.N., 1980a. Low-aspect ratio ignimbrites. Nature, London, 283: 286-287.

Walker, G.P.L., Self, S. and Froggatt, P.C., 1981a. The ground layer of the Taupo Ignimbrite: a striking example of sedimentation from a pyroclastic flow. Journal of Volcanology and Geothermal Research, 10: 1-11.

Froggatt, P.C., Wilson, C.J.N. and Walker, G.P.L., 1981. Orientation of logs in the Taupo Ignimbrite as an indicator of flow direction and vent position. Geology, 9: 109-111.

Walker, G.P.L., Wilson, C.J.N. and Froggatt, P.C., 1980b. Fines-depleted ignimbrite in New Zealand- the product of a turbulent pyroclastic flow. Geology, 8: 245-249.

Sedimentary response/aftermath

White, J.D.L., Houghton, B.F., Hodgson, K.A. and Wilson, C.J.N., 1997. Delayed sedimentary response to the A.D. 1886 eruption of Tarawera, New Zealand. Geology, 25: 459-462.

Manville, V., White, J.D.L., Houghton, B.F. and Wilson, C.J.N., 1999. Paleohydrology and sedimentology of a post-1.8 ka breakout flood from intracaldera Lake Taupo, North Island, New Zealand. Geological Society of America Bulletin, 111: 1435- 1447.

Riggs, N.R. et al., 2000. Post-1.8-ka marginal sedimentation in Lake Taupo, New Zealand: effects of wave energy and sediment supply in a rapidly rising lake. Special Publications int. Ass. Sediment., 30: 7-33.

Tongariro

Hobden, B.J., Houghton, B.F., Lanphere, M.A. and Nairn, I.A., 1996. Growth of the Tongariro volcanic complex: new evidence from K-Ar age determinations. New Zealand Journal of Geology and Geophysics, 39: 151-154.

Hobden, B.J., Houghton, B.F., Davidson, J.P. and Weaver, S.D., 1999. Small and short-lived magma batches at composite volcanoes: time windows at Tongariro volcano, New Zealand. Journal of the Geological Society, 156: 865- 868.

Hobden, B.J., Houghton, B.F. and Nairn, I.A., 2002. Growth of a young, frequently active composite cone: Ngauruhoe volcano, New Zealand. Bulletin of Volcanology.

Nairn, I.A., Kobayashi, T. and Nakagawa, M., 1998. The ~10 ka multiple vent pyroclastic eruption sequence at Tongariro Volcanic Centre, Taupo Volcanic Zone, New Zealand: Part 1. Eruptive processes during regional extension. Journal of Volcanology and Geothermal Research, 86: 19- 44.

Nakagawa, M., Nairn, I.A. and Kobayashi, T., 1998. The ~10 ka multiple vent pyroclastic eruption sequence at Tongariro Volcanic Centre, Taupo Volcanic Zone, New Zealand - Part 2. Petrological insights into magma storage and transport during regional extension. Journal of Volcanology and Geothermal Research, 86: 45- 65.

Ngauruhoe

Hobden, B.J., Houghton, B.F. and Nairn, I.A., 2002. Growth of a young, frequently active composite cone: Ngauruhoe Volcano, New Zealand. Bulletin of Volcanology.

Lube, G.; Cronin, S.J.; Platz, T.; Freundt, A.; Procter, J.N.; Henderson, C.; and Sheridan, M.F. in press. Flow and deposition of pyroclastic granular flows: a type example from the 1975 Ngauruhoe eruption, New Zealand. Submitted to Journal of Volcanology and Geothermal Research.

Nairn, I.A., 1976. Atmospheric shock waves from Ngauruhoe explosive eruptions. Nature, London, 259: 190-192.

Nairn, I.A., Hewson, C.A.Y., Latter, J.H. and Wood, C.P., 1976. Pyroclastic eruptions of Ngauruhoe volcano, central North Island, New Zealand, 1974 January and March. In: R.W. Johnson (Editor), Volcanism in Australasia. Elsevier, Amsterdam, pp. 385-405.

Self, S., 1974. Explosive activity of Ngauruhoe, 27-30 March 1974. New Zealand Journal of Geology and Geophysics, 18: 189-195.

Gregg, D.R., 1956. Eruption of Ngauruhoe 1954-1955. New Zealand Journal of Science and Technology, B37: 675-688.

Ruapehu

Hackett, W.R. and Houghton, B.F., 1989. A facies model for a Quaternary andesitic composite volcano: Ruapehu, NEw Zealand. Bulletin of Volcanology, 51: 51-68.

Gamble, J.A. et al., 1999. A fifty year perspective of magmatic evolution on Ruapehu Volcano, New Zealand: verification of open system behaviour in an arc volcano. Earth and Planetary Science Letters, 170: 301- 314.

Donoghue, S.L., Neall, V.E., Palmer, A.S. and Stewart, R.B., 1997. The volcanic history of Ruapehu during the last 2 millenia based on the record of Tufa Trig tephras. Bulletin of Volcanology, 59: 136-146.

Hackett, W.R. and Houghton, B.F., 1985. Pinnacle Ridge Member, Whakapapa Formation: a welded airfall deposit from Ruapehu volcano, Taupo Volcanic Zone. New Zealand Geological Survey Record, 8: 24-29.

Houghton, B.F., Latter, J.H. and Hackett, W.R., 1987. Volcanic hazard assessment for Ruapehu composite volcano, Taupo Volcanic Zone, New Zealand. Bulletin of Volcanology, 49: 737-751.

Houghton, B.F. and Hackett, W.R., 1984. Strombolian and phreatomagmatic deposits of Ohakune craters, Ruapehu, New Zealand: A complex interaction between external water and rising basaltic magma. Journal of Volcanological and Geothermal Research, 21: 207-231.

Houghton B.F. Bonadonna C., Thordarson, Th., Rosenberg M., Wilson C.J.N., Johnston D.M., Keyes J.R., Manville V., Sherburn, S. In prep. The 17 June 1996 eruption of Ruapehu volcano I: The anatomy of a wind-advected subplinian fall deposit

Johnston, D.M., Houghton, B.F., Neall, V.E., Ronan, K.R. and Paton, D., 2000. Impacts of the 1945 and 1995-1996 Ruapehu eruptions, New Zealand: An example of increasing societal vulnerability. Geological Society of America Bulletin, 112: 2-11.

Lecointre, J.A., Neall, V.E. and Palmer, A.S., 1998. Quaternary Lahar Stratigraphy Of the Western Ruapehu Ring Plain, New Zealand. New Zealand Journal Of Geology and Geophysics, 41: 225- 245.

Palmer, B.A. and Neall, V.E., 1989. The Murimotu Formation - 9500 year old deposits of a debris avalanche and associated lahars, Mount Ruapehu, North Island, New Zealand. New Zealand Journal of Geology and Geophysics, 32: 477-486.

(Palmer et al., 1993)Palmer, B.A., Purves, A.M. and Donoghue, S.L., 1993. Controls on accumulation of a volcaniclastic fan, Ruapehu composite volcano, New Zealand. Bulletin of Volcanology, 55: 176-189.

Ruapehu 1995-96

Johnston, D.M., Houghton, B.F., Neall, V.E., Ronan, K.R. and Paton, D., 2000. Impacts of the 1945 and 1995-1996 Ruapehu eruptions, New Zealand: An example of increasing societal vulnerability. Geological Society of America Bulletin, 112: 2-11.

Bonadonna, C.; Phillips, J.C.; Houghton, B.F. 2005. Modeling tephra fall from a Ruapehu weak plume eruption. Journal of Geophysical Research 110 B08209. 0.1029/2004JB003515.

Bonadonna, C.; Houghton, B.F. 2005. Total grain size distribution and volume of tephra-fall deposits. Bulletin of Volcanology 67:441 – 456.

Nakagawa, M., Wada, K., Thordarson, T., Wood, C.P. and Gamble, J.A., 1999. Petrologic investigations of the 1995 and 1996 eruptions of Ruapehu volcano, New Zealand: formation of discrete and small magma pockets and their intermittent discharge. Bulletin of Volcanology, 61: 15- 31.

Manville, V., Hodgson, K.A., Houghton, B.F., Keys, J.R.H. and White, J.D.L., 2000a. Tephra, snow and water: complex sedimentary responses at an active snow-capped stratovolcano, Ruapehu, New Zealand. Bulletin of Volcanology, 62: 278- 293.

Manville, V., Hodgson, K.A. and White, J.D.L., 1998. Rheological properties of a remobilised-tephra lahar associated with the 1995 eruptions of Ruapehu Volcano, New Zealand. New Zealand Journal Of Geology and Geophysics, 41: 157- 164.

Christenson, B.W., 2000. Geochemistry of fluids associated with the 1995-1996 eruption of Mt. Ruapehu, New Zealand: signatures and processes in the magmatic-hydrothermal system. Journal of Volcanology and Geothermal Research, 97: 1- 30.

Cronin, S.J., Neall, V.E., Lecointre, J.A. and Palmer, A.S., 1996. Unusual "snow slurry" lahars from Ruapehu Volcano, New Zealand, September 1995. Geology, Boulder, 24: 1107-1110.

Cronin, S.J., Neall, V.E., Lecointre, J.A. and Palmer, A.S., 1999. Dynamic interactions between lahars and stream flow: A case study from Ruapehu volcano, New Zealand. Geological Society Of America Bulletin, 111: 28- 38.

Manville, V., White, J.D.L. and Hodgson, K.A., 2000b. Dynamic interactions between lahars and stream flow: A case study from Ruapehu volcano, New Zealand: Discussion. Geological Society of America Bulletin, 112: 1149- 1151.

Cronin, S.J., Lecointre, J.A., Palmer, A.S. and Neall, V.E., 2000. Transformation, internal stratification, and depositional processes within a channelised, multi-peaked lahar flow. New Zealand Journal of Geology and Geophysics, 43: 117- 128.

Hodgson, K.A. and Manville, V.R., 1999. Sedimentology and flow behavior of a rain-triggered lahar, Mangatoetoenui Stream, Ruapehu volcano, New Zealand. Geological Society of America Bulletin, 111: 743- 754.